CMS Physics Analysis Summary

Contact: cms-pag-conveners-fsq@cern.ch 2013/04/21

Study of the properties of hard and soft particle production as a function of particle multiplicity in p-p collisions at $\sqrt{s} = 7$ TeV

The CMS Collaboration

Abstract

The characteristics of multi-particle production in p-p collisions at $\sqrt{s} = 7$ TeV are studied as a function of the event charged particle multiplicity (N_{ch}), by classifying the measured tracks into two distinct classes, those belonging to jets and those belonging to the underlying event (UE). Charged tracks are measured within pseudorapidity $|\eta| < 2.4$ and transverse momenta above $p_T = 0.25$ GeV/c, and charged-particle jets are reconstructed above $p_T = 5$ GeV/c with track-only information. The distributions of jet p_T, average p_T of UE tracks and jets, jet rates, and jet shapes are studied as a function of N_{ch} and are compared to the predictions of the PYTHIA and HERWIG Monte Carlo (MC) event generators. As the event-multiplicity increases, PYTHIA systematically predicts higher jet rates and harder p_T spectra than seen in the data, whereas HERWIG shows the opposite trend. Predictions without multi-parton interactions fail completely to describe the data. In the lowest-multiplicity events, the data show narrower jets than predicted by both MC generators.

1 Introduction

Understanding the details of multi-particle production in hadronic collisions at high energies remains an open problem in high-energy physics. At the energies of the Large Hadron Collider (LHC), experimental data are most naturally described in a picture in which an event is a combination of hadronic jets issuing from hard parton-parton interactions with exchanged momenta above O(5 GeV/c), and an underlying event from softer parton-parton interactions plus beam remnants. The production of high transverse-momentum jets, defined as collimated bunches of charged particles, is well understood from first-principles perturbative quantum chromodynamics (pQCD) as resulting from dressing of parton cascades by subsequent hadronization through soft strings stretching between final partons or formation of preconfined colorless clusters [1]. The underlying event is defined as the set of all other final-state particles that do not belong to hard hadron jets. The understanding of such a component, essentially dominated by contributions from (mini)jets, i.e. perturbative jets with relatively small transverse momenta produced in (softer) multiparton interactions (MPI) [2–9], plus soft hadronic strings from the beam remnants, is more phenomenological. In the above-described two-component approach, rare high-multiplicity events can be explained as due to a large number of MPI taking place in the p-p collision. Different variants of such a physical picture are realized in state-of-the-art Monte Carlo (MC) event generators such as PYTHIA [10, 11] and HERWIG [12]. The properties of multiparticle production turn out to be very sensitive to the assumptions made on the combination of MPI plus hard scatterings, on the modeling of the semihard multiparton interactions themselves [2], and on non-perturbative final-state effects (possible collective flow phenomena, colour reconnections, hadronization mechanism, ...).

Experimental data on multiparticle production in proton-proton collisions at LHC energies provide, however, a clear indication that our understanding of the different components contributing to the total inelastic cross section in p-p collisions at the LHC is at best incomplete. This follows, in particular, from difficulties in describing multiplicity distributions (especially their high multiplicity tails) [13] or in reproducing a new structure of the azimuthal angular correlations at 7 TeV for high multiplicity events, the so-called "ridge" [14]. Interesting data-MC disagreements were also recently reported in transverse sphericity analyses [15] and in the global event shapes [16–19]. Therefore, although the standard mixture of non-perturbative and (semi)hard physics considered by PYTHIA is sufficient for reproducing the bulk properties of minimum bias events, it fails to provide a more differential description of the data, in particular of the properties of events binned in particle multiplicity.

Our main goal is to study the characteristic features and relative importance of different mechanisms of multiparticle production in p-p collisions at 7 TeV in different multiplicity bins, i.e. at different levels of hadronic activity resulting from larger or smaller transverse overlaps of the colliding protons. Guided by the above-described physical picture we separate the particle content of each inelastic event into two subsets by identifying the jet-induced contribution and treating the rest as underlying event (UE) originating from unresolved perturbative sources such as semihard MPI and from soft stringy-type mechanisms. We compare the experimental data to the predictions of the PYTHIA 6, PYTHIA 8 and HERWIG++ 2.5 event generators.

2 Monte Carlo models

The Monte Carlo (MC) models used for comparison with the data in this analysis are the PYTHIA6 (version 6.424, tune Z2*) [10], PYTHIA8 (version 8.145, tune 4C) [20], PYTHIA8 (version 8.165, with switched-off MPI mechanism) and HERWIG++ 2.5 [12] (version UE-EE-3M) event

generators. These tunes differ in the treatment of flavor, fragmentation and in the choice of underlying event parameters including those regulating parton showers, color reconnections, cut-off values responsible for contribution from multi-parton interactions, etc. The chosen values of parameters for these tunes provide a reasonable description of the current LHC pp differential data measured in minimum bias and hard QCD processes [20]. Differences between PYTHIA and HERWIG generators include the MPI modeling – in particular PYTHIA incorporates interleaved evolution between the different scatterings, whereas HERWIG concentrates more hard scatterings in the center of the pp collision while allowing for more (disconnected) soft parton scatterings in the periphery – and the treatment of the hadronization process. Hadronization in PYTHIA is based on the Lund string model [21] while that in HERWIG++ is based on the cluster fragmentation picture in which perturbative evolution ends up in forming preconfined clusters subsequently decaying into final hadrons. The version of HERWIG++ 2.5 used includes important final-state effects due to color reconnections.

3 CMS detector

A detailed description of the CMS detector can be found in [22]. A right-handed coordinate system with the origin at the nominal interaction point (IP) is used, with the x axis pointing to the center of the LHC ring, the y axis pointing up, and the z axis oriented along the anti-clockwise beam direction. The central feature of the CMS detector is a superconducting solenoid of 6 m internal diameter providing an axial magnetic field with the nominal strength of 3.8 T. Immersed in the magnetic field are the pixel tracker, the silicon-strip tracker (SST), the lead tungstate electromagnetic calorimeter, the brass/scintillator hadron calorimeter and the muon detection system. In addition to the barrel and endcap calorimeters, the steel/quartz-fibre forward calorimeter (HF) covers the pseudorapidity region $2.9< |\eta| <5.2$, where $\eta = -\log[\tan(\theta/2)]$, and θ is the polar angle of the particle with respect to the direction of the counter-clockwise proton beam measured relative to the center of the CMS detector. Two of the CMS subdetectors acting as LHC beam monitors, the Beam Scintillation Counters (BSC) and the Beam Pick-up Timing for the experiments (BPTX) devices, were used to trigger the detector readout. The BSC's are located along the beam line on each side of the IP at a distance of 10.86 m and cover the range $3.23< |\eta| <4.65$. The two BPTX devices, which are located inside the beam pipe at the distances of 175 m from the IP, are designed to provide precise information on the structure and timing of the LHC beams with a time resolution of 0.2 ns. The tracking detector consists of 1440 silicon-pixel and 15148 silicon-strip detector modules. The barrel part consists of 3 (10) layers of pixel modules around the IP at distances ranging from 4.4 cm to 1.1 m. Five out of the 10 strip layers are double sided and provide additional z coordinate measurements. The two endcaps consist of 2 (12) disks of pixel modules that extend the pseudorapidity acceptance to $|\eta| <2.5$. The tracker provides an impact parameter resolution of about 100 mm and a transverse momentum p_{T} resolution of about 0.7% for 1 GeV/c charged particles at normal incidence.

4 Event selection and reconstruction

The present analysis uses the low-pileup data collected during the first period of 2010 (Run2010A) with proton beams at the center of mass energy of $\sqrt{s} = 7$ TeV, corresponding to integrated luminosity of$(3.18 \pm 0.14)\mathrm{pb}^{-1}$.

The data is recorded with a minimum bias trigger requiring a signal from both BPTX detectors coincident with a signal form both BSC detectors. Furthermore the position of the selected vertex is constrained to be within ± 10 cm with respect to nominal interaction point along beam

direction and 2cm in transverse direction, thereby, substantially rejecting beam-halo induced events [28]. The contamination of background events after selections in the colliding-bunch data sample was found to be negligible ($< 0.1\%$).

The fraction of events in the the data sample with pileup(two or more primary vertices per bunch crossing) varies in the range (0.4-7.8)% depending on beam condition. The fraction of events where two primary vertices are reconstructed as one, or where they share associated tracks varies within (0.04-0.2)%.

4.1 Charged tracks

The track reconstruction procedure uses information from both Pixel and SST detectors and is based on an iterative combinatorial track finder [29]. Tracks are selected for analysis if they have transverse momenta $p_{\mathrm{T}} > 0.25$ GeV/c and pseudorapidities lying within the tracker acceptance $|\eta| < 2.4$ and are associated with the primary vertex with the highest multiplicity in an event. The requirement that all tracks are associated to the primary vertex removes track coming from secondary interactions with detector materials, V^0 decays and pileup. Residual contamination from such tracks are at the level of 0.2%.

4.2 Calibration of the multiplicity

All results that use charged tracks are corrected for reconstruction inefficiencies and fake tracks. Corrections are based on two-dimensional matrices $eff(\eta, p_{\mathrm{T}})$ and $fake(\eta, p_{\mathrm{T}})$ for efficiency and fake tracks correspondingly. The true number of tracks $N^{\mathrm{true}}(\eta, p_{\mathrm{T}})$ was computed from the number of reconstructed tracks $N^{\mathrm{reco}}(\eta, p_{\mathrm{T}})$ via

$$N_{\mathrm{ch}}^{\mathrm{true}}(\eta, p_{\mathrm{T}}) = N_{\mathrm{ch}}^{\mathrm{reco}}(\eta, p_{\mathrm{T}}) \frac{1 - fake(\eta, p_{\mathrm{T}})}{eff(\eta, p_{\mathrm{T}})}\,. \tag{1}$$

The corrections for reconstruction inefficiencies and fake rates depend on track multiplicity. Four different sets of matrices $eff(\eta, p_{\mathrm{T}})$ and $fake(\eta, p_{\mathrm{T}})$ for different track multiplicity classes are used in the calibration procedure. The average efficiency is about 79–80% and the fake track rate, 3–4%. These track multiplicity classes roughly correspond to charged particle multiplicity domains (described below) used in analysis, the first three track multiplicity classes corresponding to the first three charged particle multiplicity domains and the fourth one corresponding to the fourth and fifth charged particle multiplicity domains. Such an approach results in an error of less than 0.3% for event yield versus charged particle multiplicity.

The multiplicity is defined as a number of stable (lifetime $c\tau > 10$ mm) charged particles N_{ch} with momenta $p_{\mathrm{T}} > 0.25$ GeV/c and pseudorapidities lying within $|\eta| < 2.4$. Table 1 shows the corrected charged particle multiplicity classes used in the present analysis and the number of events and mean multiplicities in each multiplicity bin after applying all event selection criteria.

4.3 Charged-particle jet reconstruction

The procedure of jet reconstruction involves two steps: (i) reconstruction of a relevant set of tracks, (ii) application of jet finding algorithm to the selected set of tracks. The analysis is based on jets that are reconstructed with charged particles only [30]. Usage of the full set of particles would lead to a significant jet energy uncertainty because of relatively large uncertainties in measuring energies of neutral particles at low p_{T} values. The jet energy uncertainty results

Multiplicity range	Mean multiplicity $\langle N_{\rm ch} \rangle$	Number of Events
Total	24.1	6 771005
$10 < N_{\rm ch} \leq 30$	18.9	2 795 688
$30 < N_{\rm ch} \leq 50$	38.8	1 271 987
$50 < N_{\rm ch} \leq 80$	61.4	627 731
$80 < N_{\rm ch} \leq 110$	90.6	105 660
$110 < N_{\rm ch} \leq 140$	119.8	11 599

Table 1: Charged-particle multiplicity domains and corresponding number of events.

in smearing of the measured $p_{\rm T}$ spectrum. The anti-k_T jet finding algorithm [25] was applied with an optimized distance parameter to separate jets from UE (see below). This algorithm is collinear- and infrared-safe and builds cone-shaped jets. The tracks are selected as an input to the jet finding algorithm if their transverse momenta satisfy $p_{\rm T} > 0.25$ GeV/c and they are associated with the primary vertex. Jets are retained if their axis lie within the fiducial region $|\eta^{\rm jetaxis}| < 1.9$, so that for a jet of effective radius of 0.5 all jet constituent tracks fall within the tracker acceptance ($|\eta| < 2.4$).

5 Analysis technique

The main purpose of this analysis is to make a detailed event-by-event study of the properties of jets and underlying event. Our approach to this problem follows the philosophy carried out in the CMS analysis of the ridge structure [24] and uses the following procedure:

- (a) Similarly to the centrality classification of events in high energy nuclear collisions, the space of events is divided into sub-ensembles characterized by charged particle multiplicities lying within a certain interval (Table 1).
- (b) In each event we identify those charged particles falling within the cones of jets at the production vertex, reconstructed with the anti-kt algorithm with radius parameter optimized to separate underlying event tracks (see below), with $p_{\rm T} > 5$ GeV/c. Hereafter charged particles falling within the cones of jets are labeled "intrajet particles".
- (c) The tracks belonging to the underlying event are defined as those left after removing all tracks within the jet cones from the total available solid angle.

In order to achieve a better separation of the contributions due to jets and underlying event, the cone radius was increased up until the UE $p_{\rm T}$ spectrum started to saturate indicating that the jet component had been effectively removed. This way of fixing the jet cone radius minimizes contamination of underlying event by jets contributions or viceversa. The UE $p_{\rm T}$-differential spectra for various values of the jet cone radius is shown in Fig. 1. We see that the parameter $R = 0.5$ is optimal. Of course, it is not possible to completely avoid mixing between jets and underlying event. To clarify the picture and minimize this mixing we measure not only the $p_{\rm T}$ spectrum of all the tracks inside cones, but also the spectrum of the leading track in each cone. For simplicity of understanding, the typical event layout is illustrated on Fig. 2.

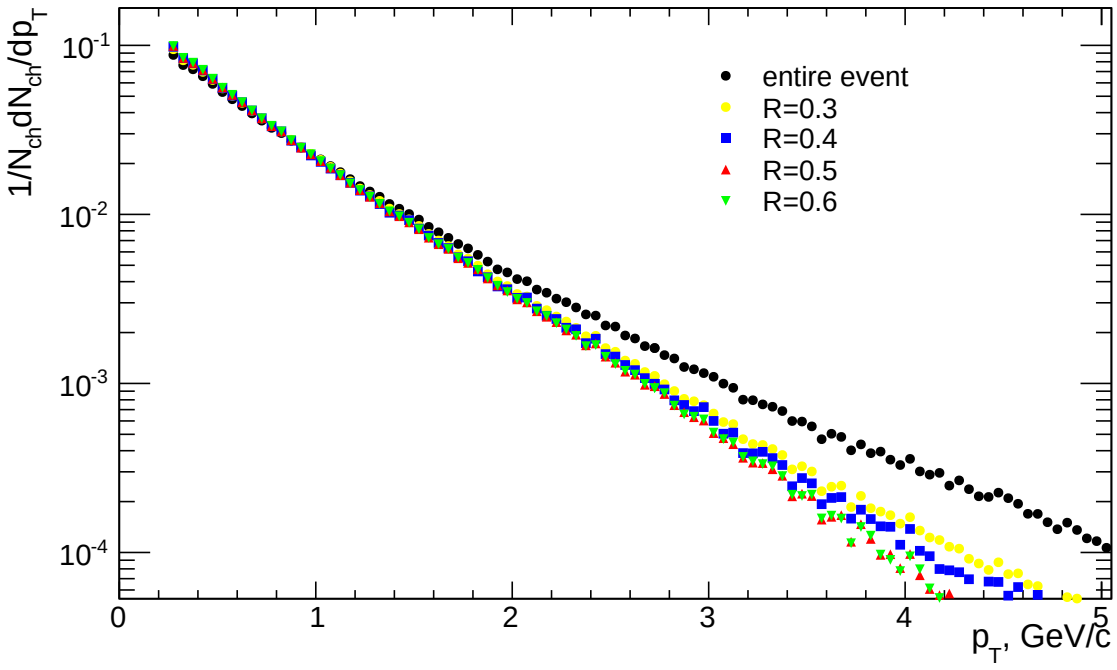

Figure 1: Dependence of p_{T} spectrum of the charged-particles of the underlying event on the radius of the jet-defining cones.

6 Data correction

6.1 Event selection corrected at particle-level

Events are selected at the stable-particle level if at least 1 charged particle is produced on each side of the interaction point within $3.23 < |\eta| < 4.65$ and, in addition, at least 5 charged particles are produced with $p_T > 0.25\,\mathrm{GeV/c}$ and$|\eta| < 2.4$. This particle-level phase space definition ensures a high trigger and event selection efficiency of $> 87\%$ for $N_{\mathrm{ch}} > 10$ and close to 100% for N_{ch} >30. The event selection efficiency is obtained using data collected a with zero-bias trigger, which requires presence of beams in the interaction point. Further, trigger conditions and event selections are imposed on these data. Final results are corrected for this event selection efficiency. Since our analysis is focused towards high-multiplicities, such an event selection has a negligible contribution from diffractive events with less hadronic activity.

6.2 Charged-particle multiplicity corrections

The charged particle multiplicity reconstruction has event-by-event fluctuations (Fig. 3, left). This leads to an event mixing between the adjacent multiplicity domains which together with a steeply falling high-multiplicity tail of the multiplicity distribution creates a migration of events toward higher multiplicities. Corrections factors are therefore obtained from comparing results at the stable-particle and detector levels of MC dataset that has been fully simulated for detector effects and then corrected for detector effects as described above (track reconstruction efficiency) and below (track-jet corrections). These corrections are applied on top of the previous ones, and account also for other possible residual effects such as different tracking performance in the dense environment (inside jets) and mixing between charged particles belonging to charged-particle jets and UE, due to misreconstruction of some jets.

Fig. 4 shows the fully-corrected distributions in each multiplicity domain for the data and MC

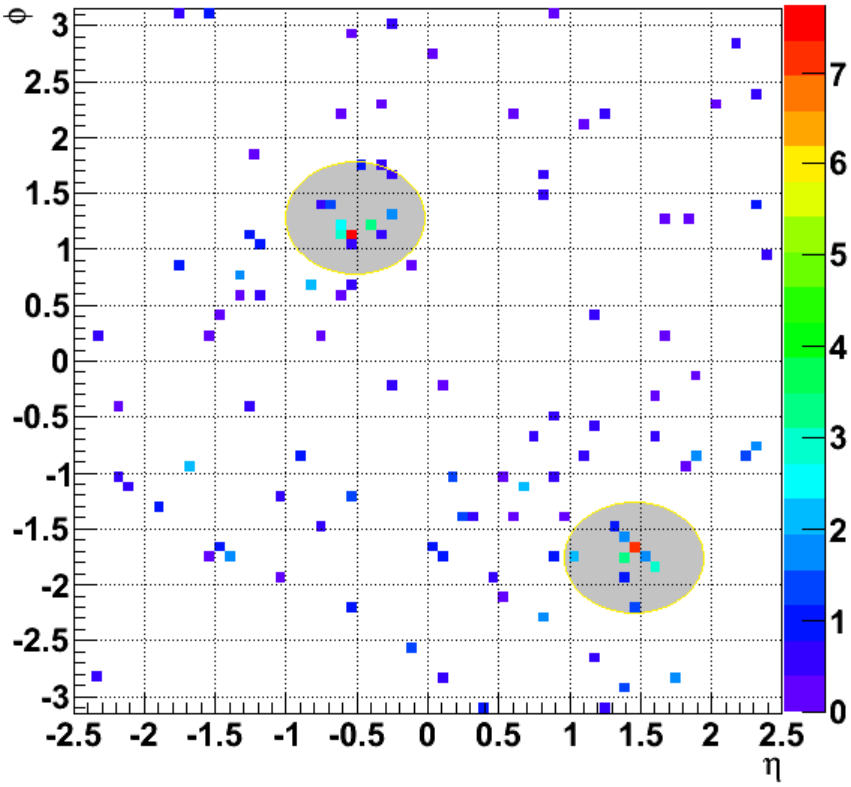

Figure 2: Event topology: small p_T color-coded rectangles represent charged particles; semi-transparent grey areas cover charged particles belonging jets. The right colored bar explains color-coding of charged particle p_T measured in (GeV/c)

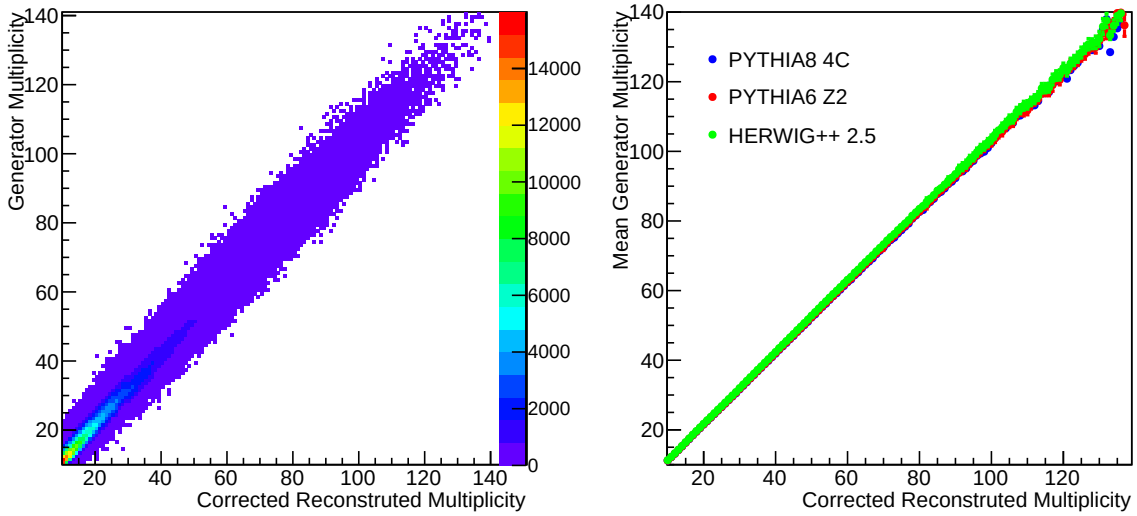

Figure 3: Charged-particle MC multiplicity versus reconstructed multiplicity corrected for detector track inefficiency and fake rate: full distribution (left), and the corresponding mean value (right).

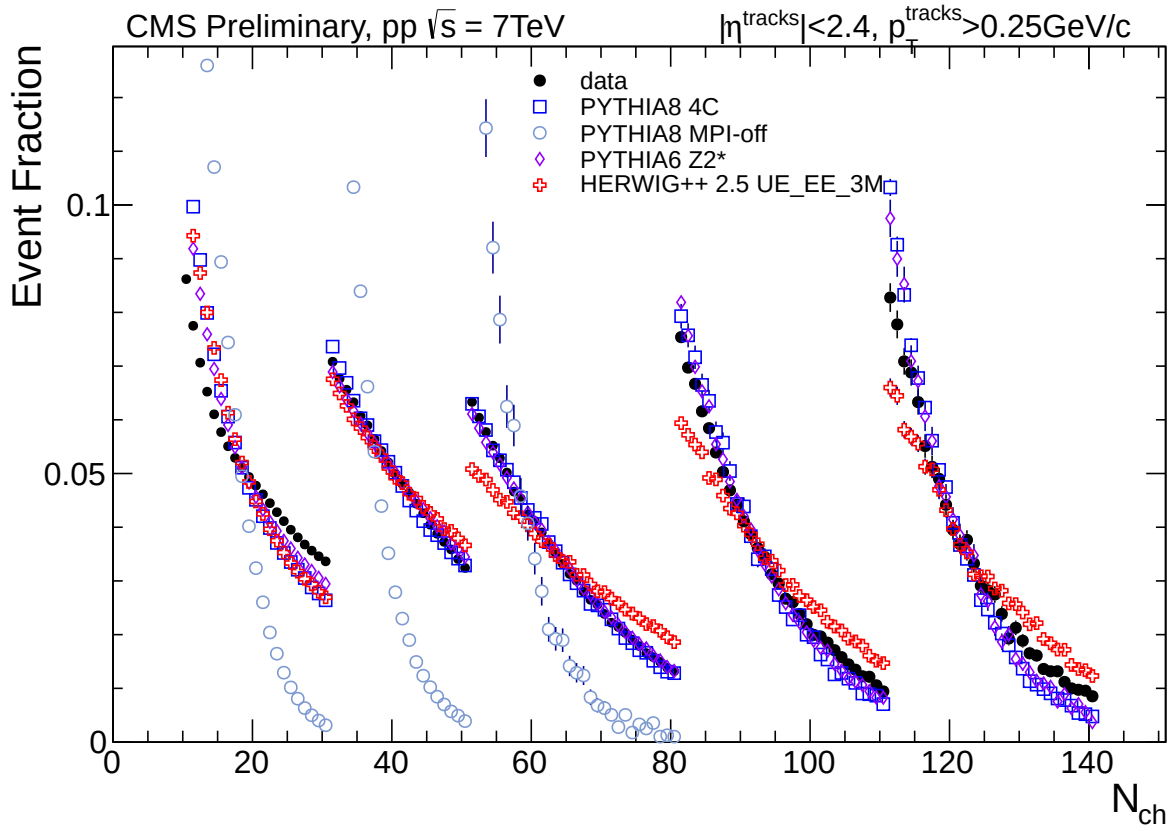

Figure 4: Charged particle multiplicity distributions for all the multiplicity bins measured in the data and compared to four MC predictions.

generators. The MC fail to describe the experimental distributions as discussed in [26]. The data-MC differences are especially severe for PYTHIA MPI-off confirming that the MPI mechanism plays a crucial role to produce large multiplicities. Since we study all event properties as a function of multiplicity, such a disagreement might introduce a bias due to different event yields at a given fixed multiplicity intervals. Reweighting the MC multiplicity distributions to bring them in agreement with the ones observed in the data results in $< 1-2\%$ corrections for all results. Final, corrected results are thus compared to the predictions obtained from the unweighted MC models."

6.3 Track-jet correction

Track-jet distributions have to be corrected for inefficiencies in the reconstruction, fake jets and for bin migrations due to the finite energy resolution. On average, a reconstructed track-jet has 95% of the energy of the original charged-particle jet. The energy resolution of such jets is about 13%. The energy response of charged-particle jets is almost independent on the p_{T} of jet. The reconstructed jet spectrum is related to the "true" one as follows:

$$M(p_{\mathrm{T}}^{\mathrm{measured}}) = \int R(p_{\mathrm{T}}^{\mathrm{measured}}, p_{\mathrm{T}}^{\mathrm{true}}) T(p_{\mathrm{T}}^{\mathrm{true}}) dp_{\mathrm{T}}^{\mathrm{true}}, \tag{2}$$

where $M(p_{\mathrm{T}}^{\mathrm{measured}})$ and $T(p_{\mathrm{T}}^{\mathrm{true}})$ are measured and true p_{T} spectra respectively and $R(p_{\mathrm{T}}^{\mathrm{measured}}, p_{\mathrm{T}}^{\mathrm{true}})$ is a response function obtained from the Monte Carlo. In application to real data the integral in

Eq. (2) turns into summation over discrete values of p_{T}. The problem of inverting the response relation is well known and was extensively studied in literature. In our analysis the iterative Bayesian unfolding procedure [31] is applied. Since jet properties and, consequently, detector response change with multiplicity, individual response matrices are used in each multiplicity domain.

These above described issues of measurement of charged-particle jet p_{T} spectrum are corrected for in the following order:

1. First, the reconstructed p_{T} spectrum is corrected for fake jets, since their energy is a measured quantity.
2. Unfolding procedure is applied to correct for instrumental effects linked to jet energy scale and resolution.
3. Since jet reconstruction efficiency is a function of "true" jet p_{T}, the correction for not reconstructed jets is applied at final step.

7 Systematics uncertainties

The following sources of systematic uncertainties are considered:

1) **Events selection efficiency:** The event selection efficiency can be estimated in two ways. The first one uses data collected with a zero-bias trigger, which requires presence of beams in the interaction point. Further, any trigger conditions and event selections can be imposed on these data. The second one is fully based on MC simulation. The differences between both methods are assigned as a systematic error.

2) **Association of tracks with primary vertex(track selection):** Tracks that are coming from a non-primary interactions result in the wrong multiplicity classification of event and bias the event properties at a given multiplicity. These tracks originate from secondary interactions with detector material, V^0 decays and pileup. Moreover these tracks can bias the p_{T} spectrum of primary tracks. As it is not possible to completely avoid contamination by such tracks, the stability of the results has been estimated by tightening and loosening the association criteria. Removing contamination inevitably leads to rejection of some valid primary tracks, so for each set of the association criteria a special efficiency and fake rate correction must be used.

3) **Tracking performance:** A correct description of the tracking performance in the Monte Carlo simulation of the detector is essential. A conservative estimate of the uncertainty of this efficiency of 2.3% is taken from [23].

4) **Model dependence of correction procedures:** Different MC models can show slightly different detector and reconstruction responses. Two models, PYTHIA 6 tune Z2* and PYTHIA 8 tune 4C are used to compute tracking and jet performance and correction factors. Corrections based on the PYTHIA 6 tune Z2* model, which provides a better agreement with data, are used to get the central values of different physics quantities. The differences between these two methods are assigned as systematic uncertainty.

5) **Unfolding of jet p_{T} spectrum:** The unfolding procedure used to correct for bin migrations in jet p_{T} spectra is based on an iterative "Bayesian" method [31] for which we find that 4–5 iterations are optimal. Varying number of iterations (± 1 with respect to the optimal value) and the reco-generated jet matching parameter ($0.15 < \Delta R < 0.25$) leads to systematic uncertainty

Table 2: Summary of systematic and statistical uncertainties, and their sum in quadrature (bottom row).

source of uncertainty	$\langle p_{\mathrm{T}}^{fullevent} \rangle$	$\langle p_{\mathrm{T}}^{UE} \rangle$	$\langle p_{\mathrm{T}}^{intrajet} \rangle$	$\langle p_{\mathrm{T}}^{intrajetleader} \rangle$	$\rho(R)$
event selection	$< 0.1\%$	$< 0.1\%$	$< 0.1\%$	$< 0.1\%$	$< 0.3\%$
track selection	$< 0.2\%$	$< 0.2\%$	$< 0.2\%$	$< 0.4\%$	$< 1\%$
tracking performance	$< 0.3\%$	$< 0.3\%$	$< 0.4\%$	$< 0.4\%$	$< 4\%$
model dependence	$< 0.5\%$	$< 0.4\%$	$< 0.5\%$	$< 0.5\%$	$< 5\%$
statistical	$< 0.1\%$	$< 0.1\%$	$< 0.2\%$	$< 0.4\%$	$2 - 8\%$
total	$0.5 - 0.7\%$	$0.5 - 0.6\%$	$0.5 - 0.7\%$	$< 0.9\%$	$4 - 9\%$ rises with R and multiplicity

Table 3: Summary of systematic and statistical uncertainties, and their sum in quadrature (bottom row).

source of uncertainty	ch. jet p_{T} spectrum	ch. jet rate ($p_{\mathrm{T}} > 5GeV/c$)	ch. jet rate ($p_{\mathrm{T}} > 30GeV/c$)	$\langle p_{\mathrm{T}}^{ch.jet} \rangle$
event selection	$< 2\%$	$< 2\%$	$< 2\%$	$< 0.1\%$
track selection	$< 1\%$	$< 2\%$	$< 4\%$	$< 0.1\%$
tracking performance	$< 3\%$	2%	$< 5\%$	$< 0.5\%$
model dependence	$< 3\%$	2%	$< 6\%$	$< 0.4\%$
unfolding	3%	$< 2\%$	$< 3\%$	$< 0.2\%$
statistical	$1 - 8\%$ ($p_{\mathrm{T}}^{\mathrm{ch.jet}} < 25\,\mathrm{GeV}/c$) $10 - 40\%$ ($p_{\mathrm{T}}^{\mathrm{ch.jet}} > 25\,\mathrm{GeV}/c$)	$< 1\%$	$< 9\%$	$< 0.4\%$
total	$4 - 10\%$ ($p_{\mathrm{T}}^{\mathrm{ch.jet}} < 25\,\mathrm{GeV}/c$) $10 - 40\%$ ($p_{\mathrm{T}}^{\mathrm{ch.jet}} > 25\,\mathrm{GeV}/c$)	$< 5\%$	$< 12\%$	0.8%

of $(0.5 - 2)\%$. These errors propagate to $< 0.2\%$ error on the average p_T of jet spectrum, and $< 2\%$ for charged-particle jet rates.

6) **Pileup:** The analysis uses low-pileup data taken in 2010 ($Run2010A$). Nevertheless, rare high multiplicity events might be the result of overlapping pp collisions in same bunch-crossing. Possible effect of pileup is estimated comparing results at different instantaneous bunch-crossing luminosities. The differences found between these subsets are of order of the statistical uncertainties of the sample. The dependence of instantaneous bunch-crossing luminosity on charged particle multiplicity shows no dependence on the charged particle multiplicity, meaning that high-multiplicity events are not effectively affected by pileup.

Tables 2, 3 summarize the systematic and statistical uncertainties of all the measured quantities. The total uncertainties are the quadrature sum of the individual systematic and statistical uncertainties. The total uncertainties on jet p_{T} spectra are of order of 4-8% up to $p_{\mathrm{T}} \approx 25$ GeV/c, and for $p_{\mathrm{T}} > 25$ GeV/c statistical uncertianty being dominant.

Table 4: Average transverse momentum for different types of charged particles (inclusive, intra-jet, underlying event) and charged-particle jets, and charged-particle jet rates (above $p_{\mathrm{T}} > 5$ GeV/c) measured in p-p collisions at 7 TeV in different classes of events characterized by their charged-particle multiplicity and compared to the predictions of 3 MCs event generators. Note: Not shown uncertainties are smaller than last digit of corresponding value.

	$\langle p_{\mathrm{T}}^{\mathrm{track}} \rangle$, GeV/$c$	$\langle p_{\mathrm{T}}^{\mathrm{ij}} \rangle$, GeV/$c$	$\langle p_{\mathrm{T}}^{\mathrm{ue}} \rangle$, GeV/$c$	$\langle p_{\mathrm{T}}^{\mathrm{ch.jet}} \rangle$	$\langle \frac{\#\mathrm{jets}}{\mathrm{event}} \rangle$
$10 < N \leq 30$					
Data	0.68 ± 0.01	1.90 ± 0.02	0.65 ± 0.01	6.86 ± 0.06	0.053 ± 0.004
PYTHIA8 4C	0.67	1.83	0.64	7.08 ± 0.01	0.075
PYTHIA6 Z2*	0.67	1.86	0.65	7.01 ± 0.01	0.067
HERWIG++ 2.5	0.68	1.81	0.65	6.92 ± 0.01	0.095
$30 < N \leq 50$					
Data	0.75 ± 0.01	1.64 ± 0.02	0.71 ± 0.01	7.04 ± 0.09	0.283 ± 0.012
PYTHIA8 4C	0.77	1.62	0.72	7.26 ± 0.01	0.386
PYTHIA6 Z2*	0.74	1.62	0.70	7.20 ± 0.01	0.304
HERWIG++ 2.5	0.72	1.62	0.68	7.02 ± 0.01	0.375
$50 < N \leq 80$					
Data	0.80 ± 0.01	1.45 ± 0.01	0.74 ± 0.01	7.18 ± 0.09	0.84 ± 0.03
PYTHIA8 4C	0.84	1.49	0.76	7.41 ± 0.01	1.09
PYTHIA6 Z2*	0.80	1.44	0.74	7.30 ± 0.01	0.87
HERWIG++ 2.5	0.74	1.43	0.68	7.10 ± 0.01	0.88
$80 < N \leq 110$					
Data	0.85 ± 0.01	1.32 ± 0.01	0.76 ± 0.01	7.47 ± 0.11	2.11 ± 0.09
PYTHIA8 4C	0.90	1.41	0.78	7.77 ± 0.02	2.54
PYTHIA6 Z2*	0.85	1.33	0.76	7.64 ± 0.01	2.12
HERWIG++ 2.5	0.74	1.28	0.66	7.25 ± 0.01	1.66
$110 < N \leq 140$					
Data	0.88 ± 0.01	1.24 ± 0.01	0.77 ± 0.01	7.82 ± 0.11	3.66 ± 0.14
PYTHIA8 4C	0.95	1.36	0.79	8.31 ± 0.03	4.46
PYTHIA6 Z2*	0.90	1.29	0.77	8.15 ± 0.02	3.95
HERWIG++ 2.5	0.70	1.16	0.62	7.37 ± 0.01	2.41

8 Results

8.1 General properties of charged particles from jets and from UE

We start with discussing general properties of high- and low-multiplicity domains using five charged particle intervals. Table 4 lists all the measured quantities for the charged-particle jets and UE compared with the predictions from PYTHIA8 tune 4C, PYTHIA8 MPI-off, PYTHIA6 tune Z2* and HERWIG++ 2.5. For each multiplicity class, we show the fully-corrected results for the mean transverse momenta of all tracks $\langle p_{\mathrm{T}}^{\mathrm{track}} \rangle$, intrajet tracks $\langle p_{\mathrm{T}}^{\mathrm{ij}} \rangle$ and UE tracks $\langle p_{\mathrm{T}}^{\mathrm{UE}} \rangle$ components, the mean transverse momentum of charged-particle jets $\langle p_{\mathrm{T}}^{\mathrm{ch.jet}} \rangle$ and the average number of jets per event $\langle \frac{\#\mathrm{jets}}{\mathrm{event}} \rangle$. The charged particles are selected with $|\eta| < 2.4$ and $p_{\mathrm{T}} > 0.25$ GeV/c, and charged-particle jets with $|\eta| < 1.9$ and $p_{\mathrm{T}} > 5$ GeV/c.

The dependencies of the mean transverse momenta of charged tracks on multiplicity for full events, jets and underlying events (first three columns of Table 4) are shown in Figs. 5–7. From Figs. 5 and 6, we see that the approximately logarithmic dependence of the mean transverse momentum of charged particles as a function of multiplicity in total and underlying events is

well described by both PYTHIA tunes, especially by PYTHIA6 tune Z2*, is not properly described by HERWIG++, and it is completely missed by PYTHIA8 without MPI. Both PYTHIA tunes predict somewhat larger values of mean p_{T} starting from the second multiplicity bin with the difference between MC predictions and data growing with multiplicity. The deviation from the data is, however, quite small, especially for PYTHIA6 tune Z2*. HERWIG++ shows a mean p_{T} that does not logarithmically rise with N_{ch} but that decreases beyond $N_{\mathrm{ch}} \approx 60$.

From Figs. 7–8 it is clear that the N_{ch}-dependence of the transverse momenta of intrajet constituents and leading-track of the jet shows the opposite behaviour compared to those from the global and underlying events (Figs.5–6) and decreases logarithmically with increasing multiplicities. Part of the decrease of intrajet average p_{T} with multiplicity could be due to extra soft UE contributions falling within the jet cone (which go up from about 5% for $N_{\mathrm{ch}} \approx 20$, to about 20% for $N_{\mathrm{ch}} \approx 130$) but this is clearly not the only effect as the leading-tracks of the jets have on average also a smaller transverse momentum. In terms of data-MC comparisons, we see that the PYTHIA6 tune Z2* describes data quite well and somewhat better than HERWIG++. PYTHIA8 tune 4C produces harder intrajet charged particle spectrum at high multiplicities, and PYTHIA8 (MPI-off) again completely misses the data. For the leading-track in the jet there is s a systematic difference between PYTHIA8 tune 4C, PYTHIA6 tune Z2* and HERWIG++ 2.5 and the data such that the MC tend to underestimate the mean transverse momentum of leading charged particles at small multiplicities and overestimate it at large ones. PYTHIA8 without MPI shows a too strong increase of $\langle p_{\mathrm{T}}^{\mathrm{leading-track}} \rangle$ with N_{ch}. As multiplicity rises it enriches events with hard partons only, whereas the standard PYTHIA MC (with MPI) includes additional semi-hard parton interactions in addition to the primary parton interaction which soften the p_{T} spectra.

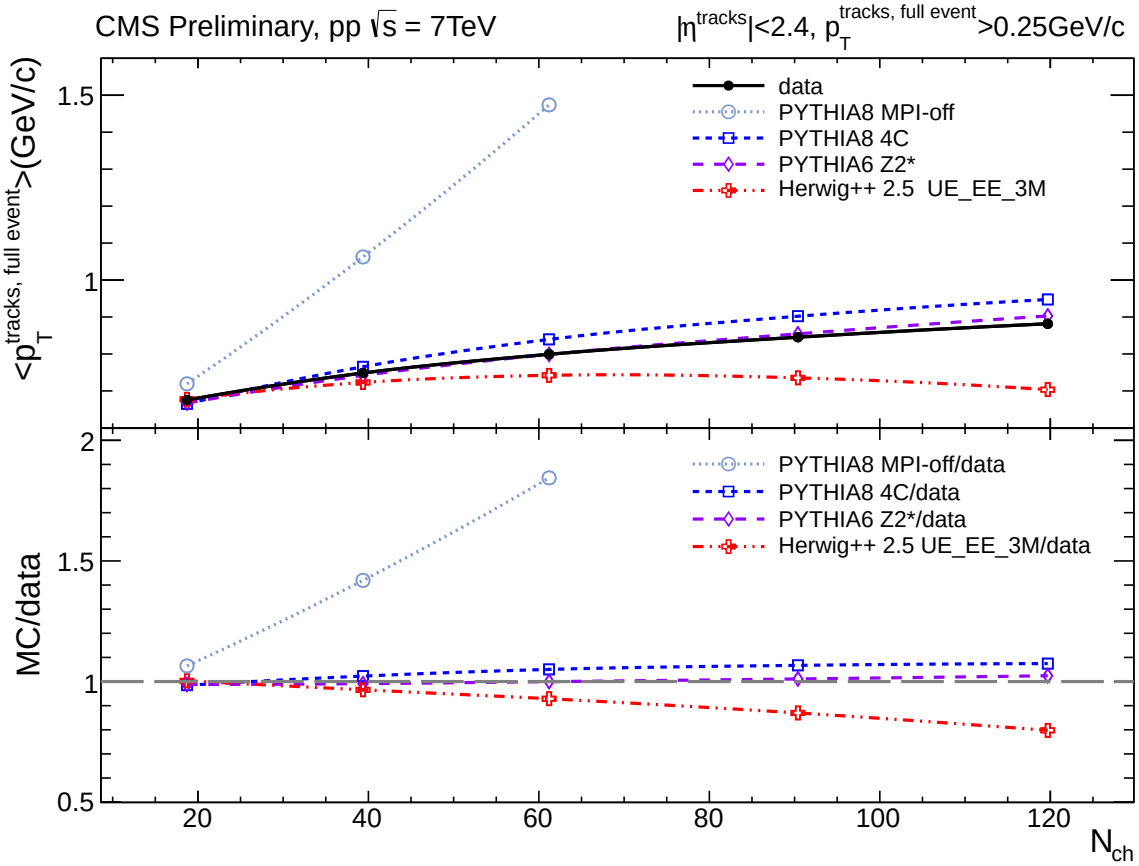

Figure 5: Mean transverse momentum of inclusive charged tracks with $p_{\mathrm{T}} > 0.25$ GeV/c versus the p-p charged-particle multiplicity (N_{ch} within $|\eta| < 2.4$), full events in p-p collisions at 7 TeV.

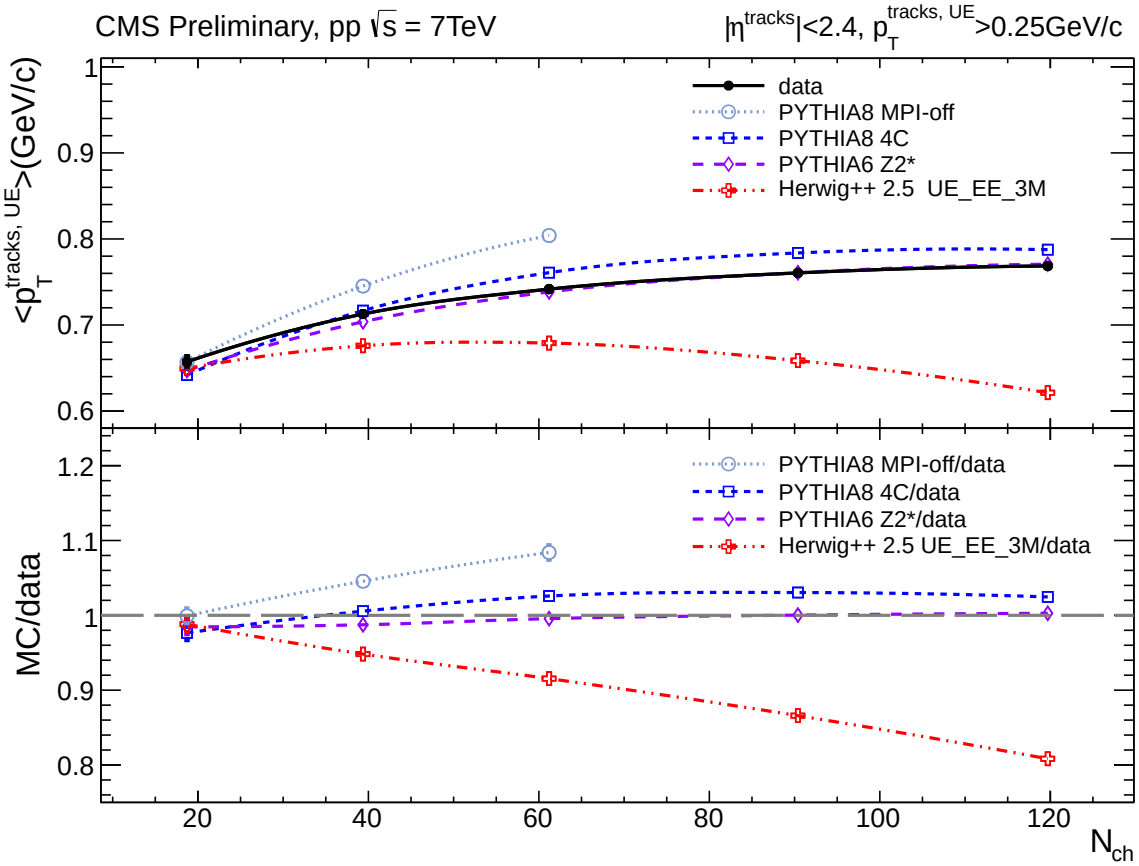

Figure 6: Mean transverse momentum of charged tracks with $p_{\mathrm{T}} > 0.25$ GeV/c versus charged-particle multiplicity (N_{ch} within $|\eta| < 2.4$), underlying events in p-p collisions at 7 TeV.

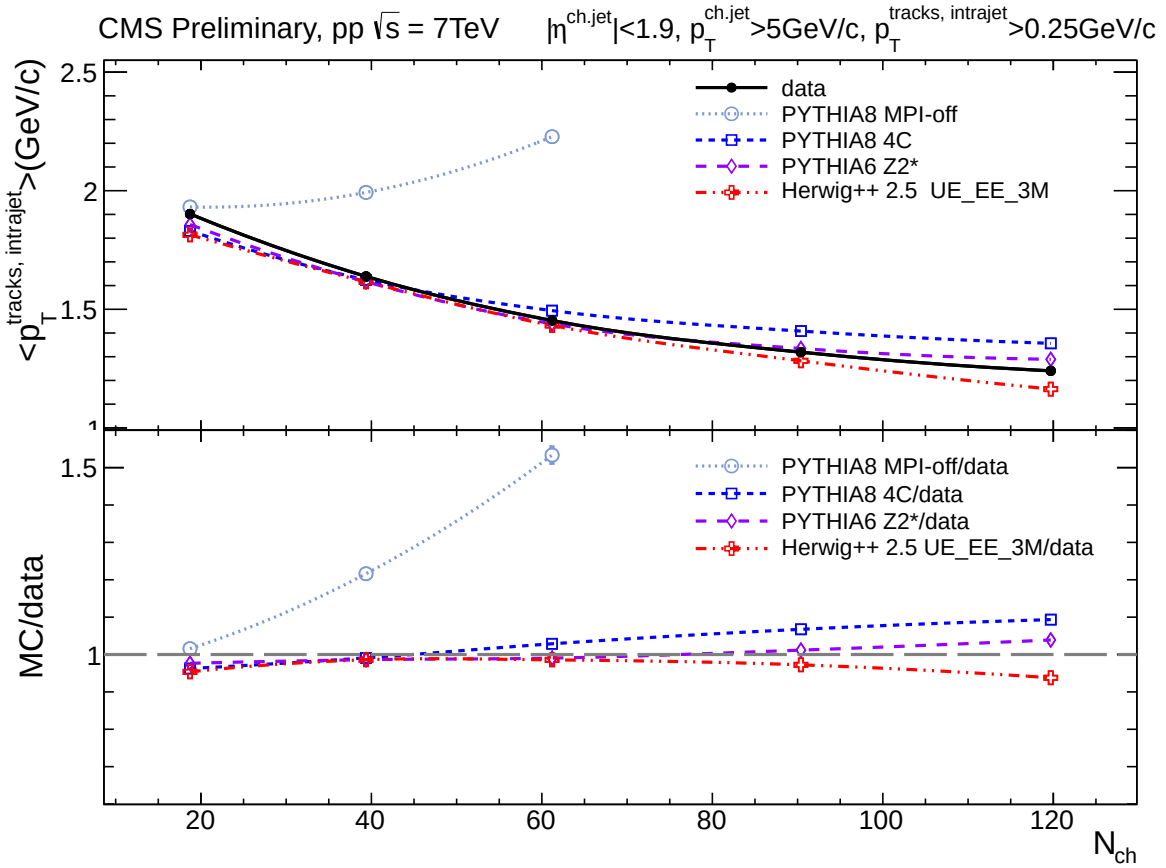

Figure 7: Mean transverse momentum of intrajet charged tracks with $p_{\mathrm{T}} > 0.25$ GeV/c versus charged-particle multiplicity (N_{ch} within $|\eta| < 2.4$) in p-p collisions at 7 TeV.

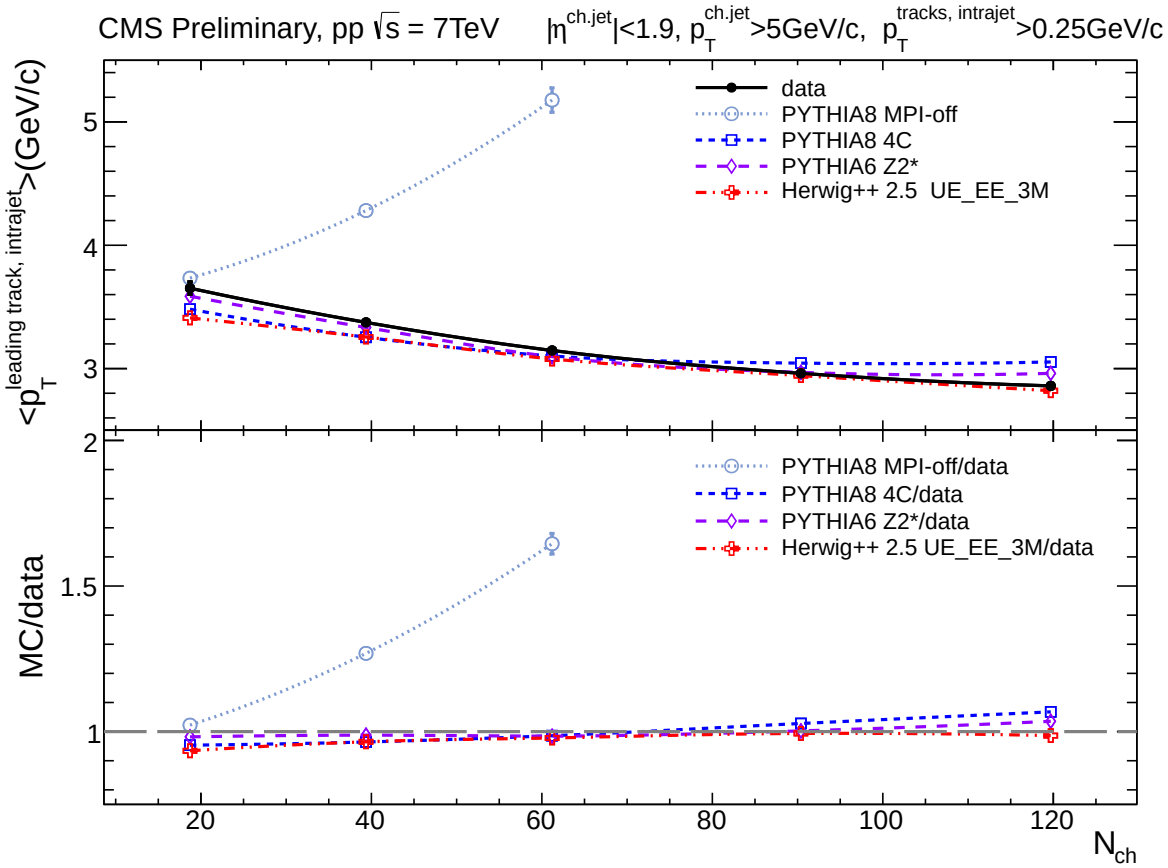

Figure 8: Mean transverse momentum of leading intrajet charged tracks with $p_{\mathrm{T}} > 0.25$ GeV/c versus charged-particle multiplicity (N_{ch} within $|\eta| < 2.4$) in p-p collisions at 7 TeV.

8.2 Charged-particle jets properties

In the previous section the jet substructure was investigated via properties of intrajet and leading particles. Now we turn to the description of the multiplicity-dependent properties of jets as such. The generic properties of inclusive jet production, integrated over all multiplicities (i.e. dominated by events with moderately low multiplicities), are described quite well by QCD MC models [27]. Here, we concentrate on the multiplicity dependence of such characteristics as a number of jets per event, their mean transverse momenta, differential-p_{T} spectra, as well as their widths.

Our study is closely related to recent results on the global event shapes. In particular, some anomalies in the event shape variables at high multiplicities in pp-collisions have been noticed by the ALICE collaboration [15, 16]. The transverse sphericity is found to grow with multiplicity whereas MC generators predict the opposite trend. However, the corresponding multiplicities are much lower there than in the present study because of the smaller rapidity coverage $|\eta| < 0.8$ in the data of [15, 16]. Some indications on this effect are also seen in the latest ATLAS publication [17] even though in its earlier results [18], as well as in the CMS analysis [19] no serious disagreement with MC generators was found because they did not separate events by multiplicity. We show here that the higher sphericity of high-multiplicity events compared to MC predictions is due to an apparent reduction of the relative jet yields in such type of events.

8.2.1 Charged-particle jet production rates

The multiplicity-dependence of the per-event number of jets with jet transverse momentum exceeding a given threshold, $p_{\mathrm{T}}^{\mathrm{ch.jet}} > p_{\mathrm{T}}^{*}$ with $p_{\mathrm{T}}^{*} = 5$ GeV/c and $p_{\mathrm{T}}^{*} = 30$ GeV/c, is displayed in Figs. 9 and 10 respectively.

For the small cutoff of 5 GeV/c the data increase from an average 0.5 jets/event to about 4 jets/event going from the lowest to the highest charged-particle multiplicity. Such results are very well described by PYTHIA6 tune Z2*, while predictions of PYTHIA8 tune 4C overestimate the rates at all N_{ch} and HERWIG 2.5 underestimates them for increasing N_{ch}. For the higher 30 GeV/c cutoff, a large disagreement with the data is found in the higher multiplicity bins (Fig. 10), where both versions of PYTHIA predict a factor of two more jets than seen in the data. HERWIG, on the contrary, predicts a factor of 10 *less* jet rates than experimentally measured. The prediction from PYTHIA8 without MPI contributions is completely off-scale (by factors of 3.5–6) and not shown in the plots.

The analysis of the multiplicity-dependence of the mean transverse momentum of charged-particle jets $\langle p_{\mathrm{T}}^{\mathrm{ch.jet}} \rangle$ is shown in Fig. 11. The average $\langle p_{\mathrm{T}}^{\mathrm{ch.jet}} \rangle$ increases slowly with N_{ch} from about 7 to 7.7 GeV/c^2. PYTHIA8 tune 4C, PYTHIA6 tune Z2* and HERWIG++ 2.5 are in good agreement with the data at low and intermediate multiplicities but display an increasingly higher value of $\langle p_{\mathrm{T}}^{\mathrm{ch.jet}} \rangle$ up to 8.4 GeV/c^2 in the highest-multiplicity events.

8.2.2 Charged-particle jet spectra

A more detailed picture of the properties of jet p_{T} spectra in the data and MC predictions is provided by the comparison of the p_{T}-differential spectra in each one of the five multiplicity bins shown in Figs. 12–16. In the first three multiplicity domains the measured jet p_{T} spectra are reasonably well reproduced by the MC predictions. However, in the two highest multiplicity bins $80 < N_{\mathrm{ch}} \leq 110$ (Fig. 15) and $110 < N_{\mathrm{ch}} \leq 140$ (Fig. 16) we observe much softer jet p_{T} spectra at transverse momenta $p_{\mathrm{T}} > 20$ GeV, where the suppression factor goes beyond $\sim$2 with respect to PYTHIA predictions. On the contrary, HERWIG tends to produce too soft

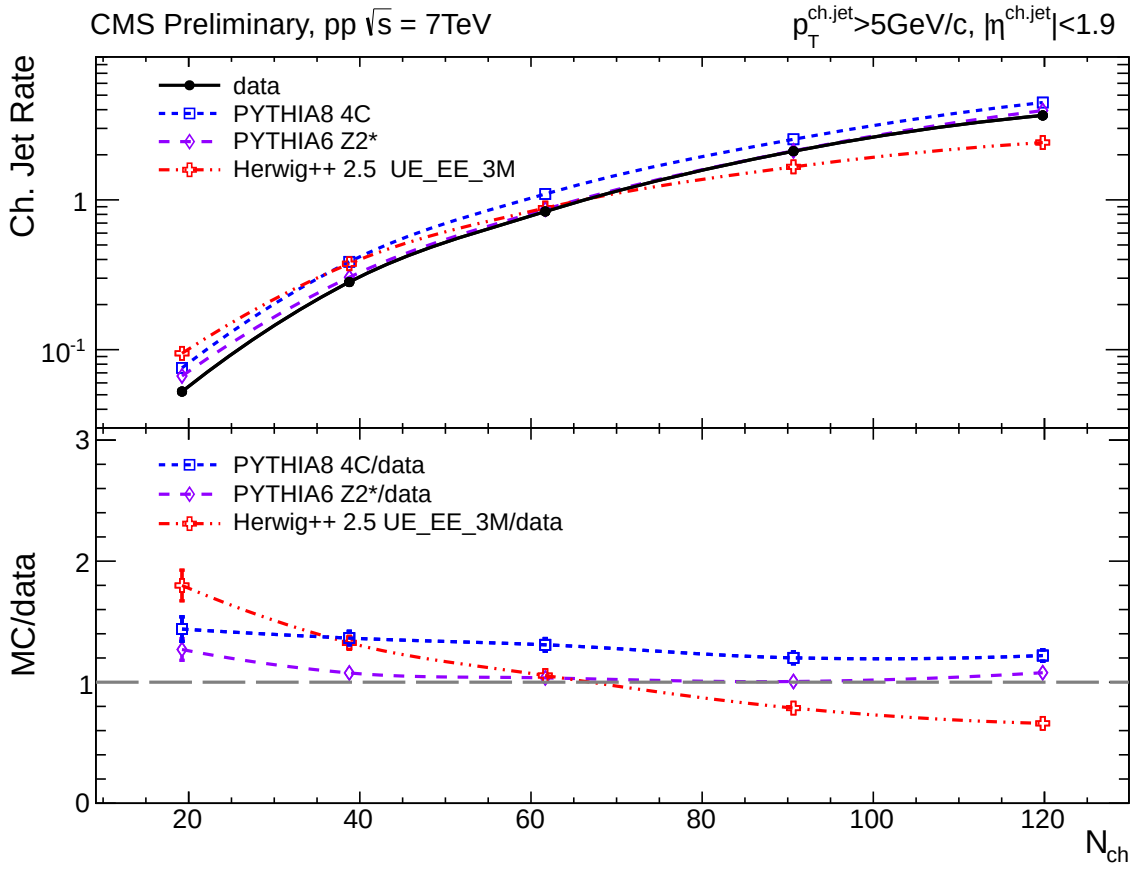

Figure 9: Number of charged-particle jets per event for threshold $p_{\mathrm{T}}^{\mathrm{ch.jet}} > 5$ GeV/c and axes lying within $|\eta| < 1.9$ versus charged-particle multiplicity (N_{ch} within $|\eta| < 2.4$) in p-p collisions at 7 TeV. Error bars denote the total uncertainties.

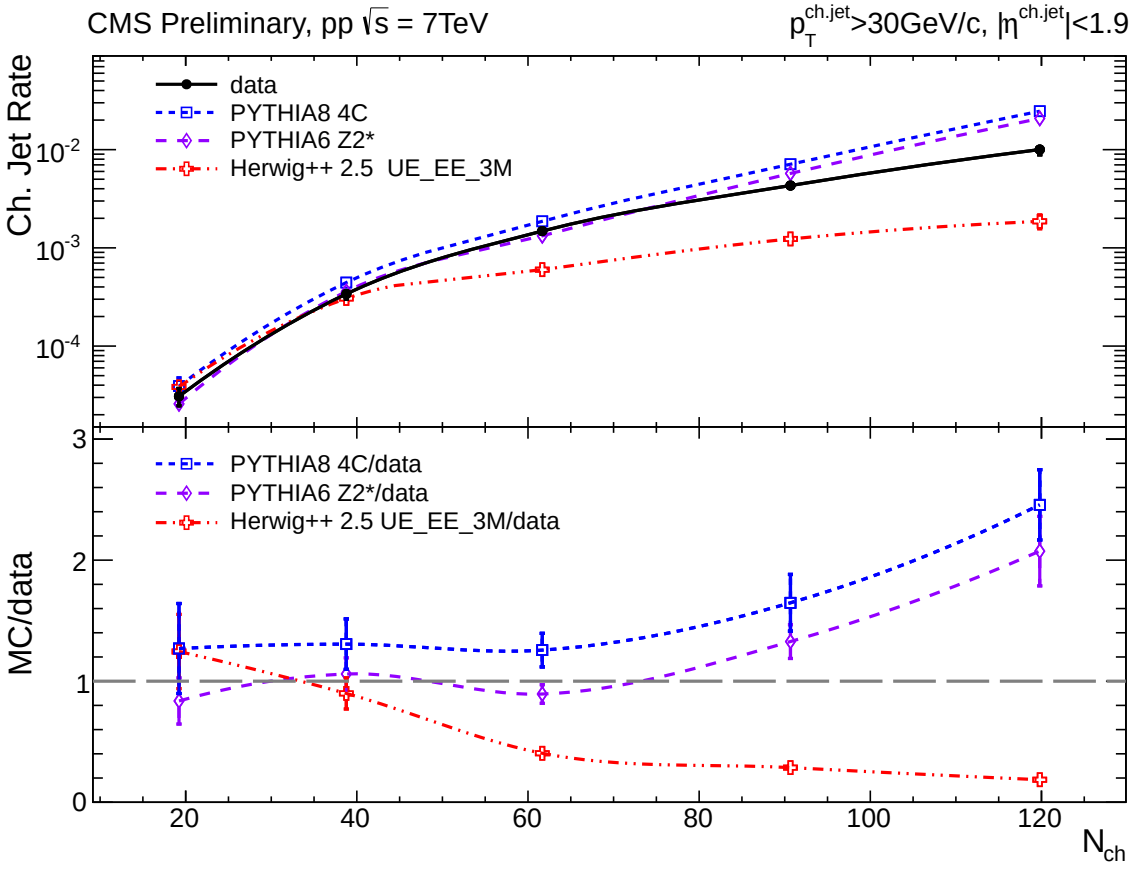

Figure 10: Number of charged-particle jets per event for threshold $p_{\mathrm{T}}^{\mathrm{ch.jet}} > 30$ GeV/c and axes lying within $|\eta| < 1.9$ versus charged-particle multiplicity (N_{ch} within $|\eta| < 2.4$) in p-p collisions at 7 TeV. Error bars denote the total uncertainties.

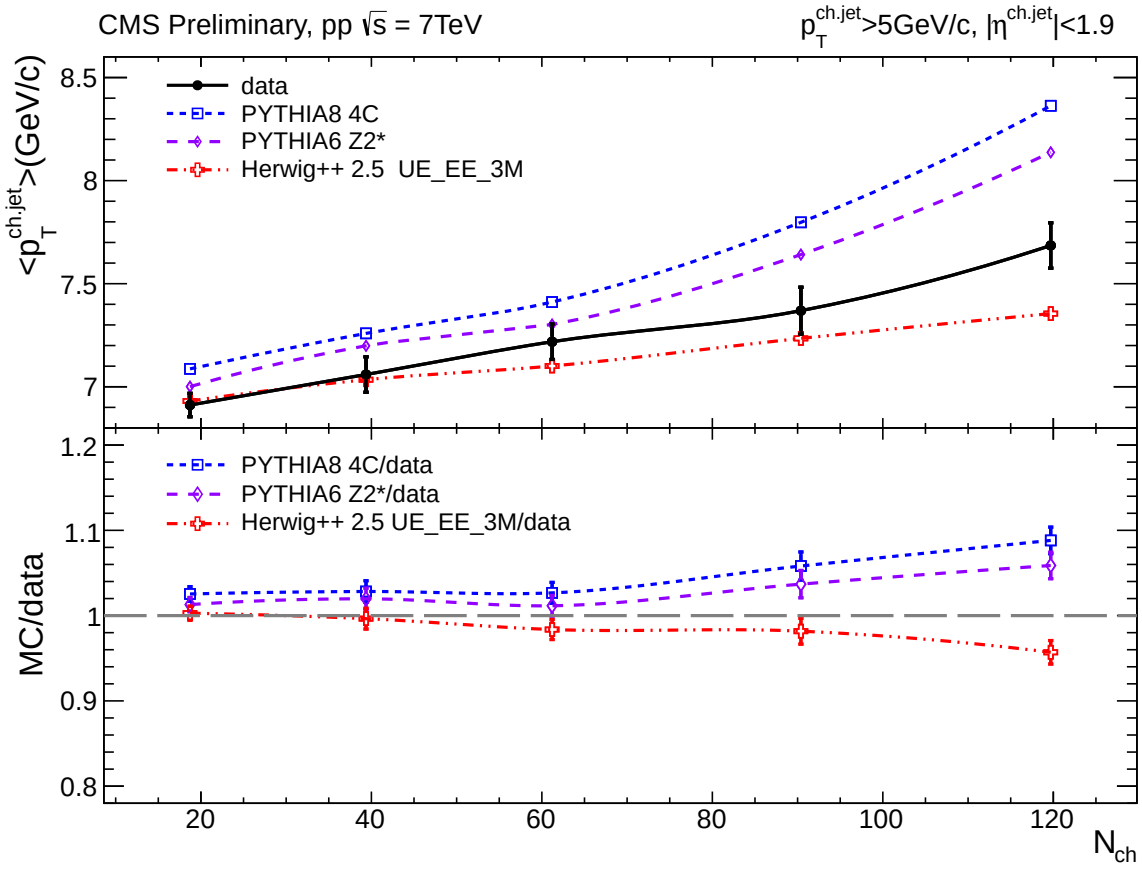

Figure 11: Mean transverse momentum of charged-particle jets (with $p_{\mathrm{T}}^{\mathrm{ch.jet}} > 5$ GeV/c and axes within $|\eta| < 1.9$) versus charged-particle multiplicity (N_{ch} within $|\eta| < 2.4$) in p-p collisions at 7 TeV.

charged-particle jets in all multiplicity domains. The observed "softening" of the jet spectra compared to PYTHIA, explains also the higher sphericity of large-multiplicity events observed in [15, 16].

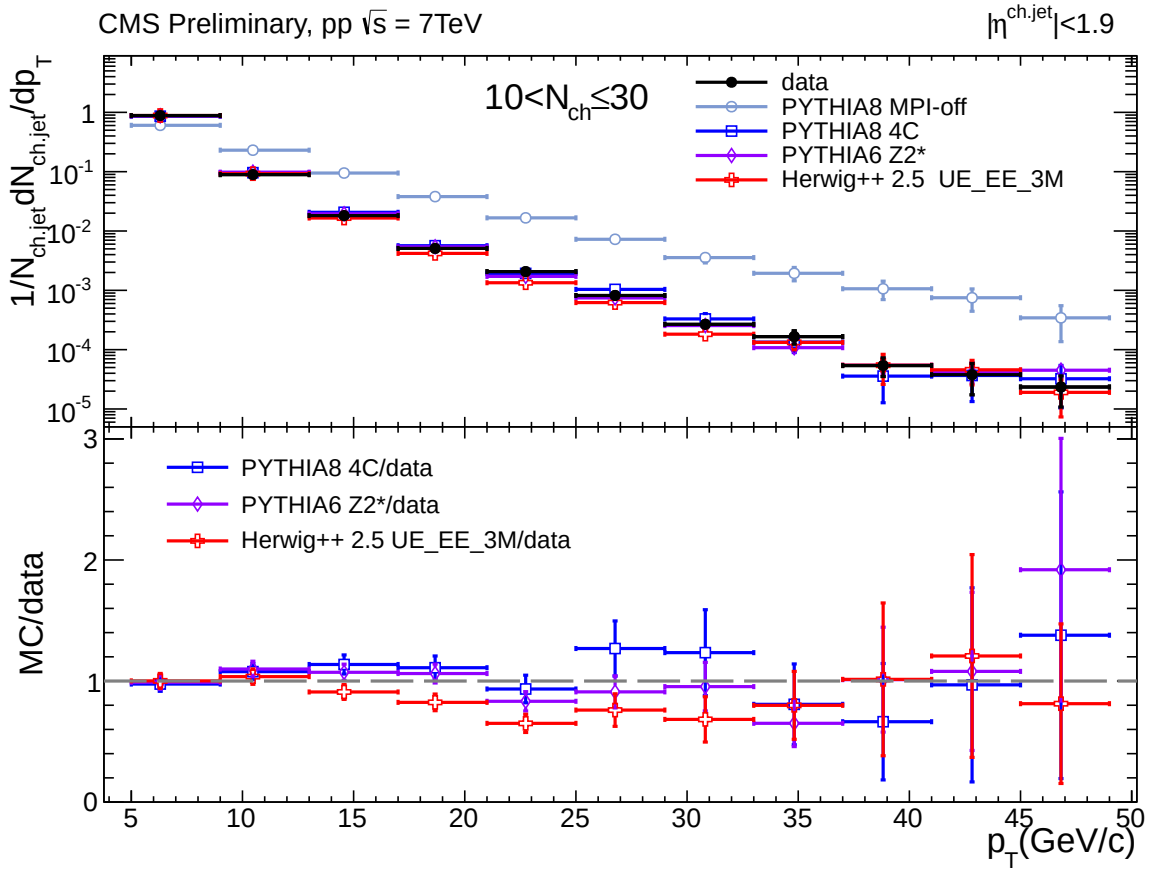

Figure 12: Inclusive charged-particle jet p_{T} spectrum in the multiplicity domain $10 < N_{\mathrm{ch}}(|\eta| < 2.4) \leq 30$ in p-p collisions at 7 TeV.

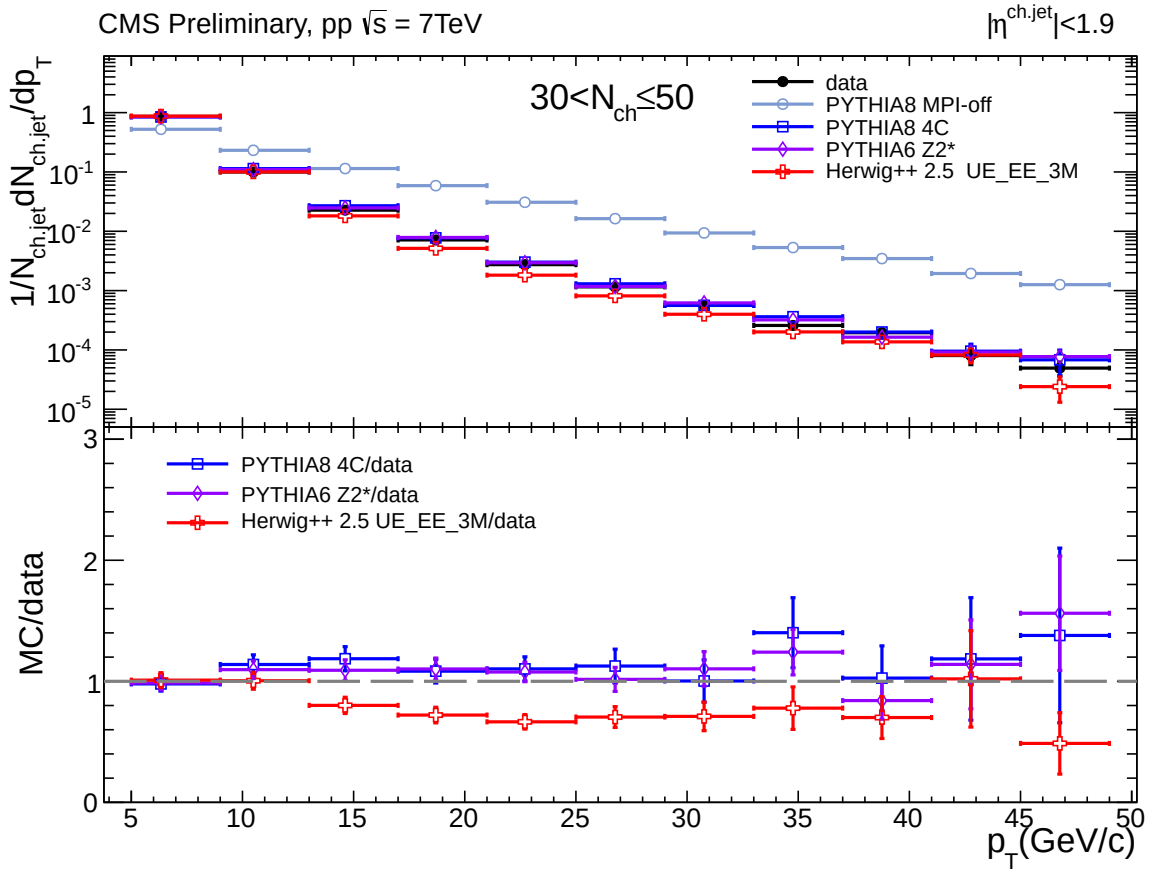

Figure 13: Inclusive charged-particle jet p_{T} spectrum in the multiplicity domain $30 < N_{\mathrm{ch}}(|\eta| < 2.4) \leq 50$ in p-p collisions at 7 TeV.

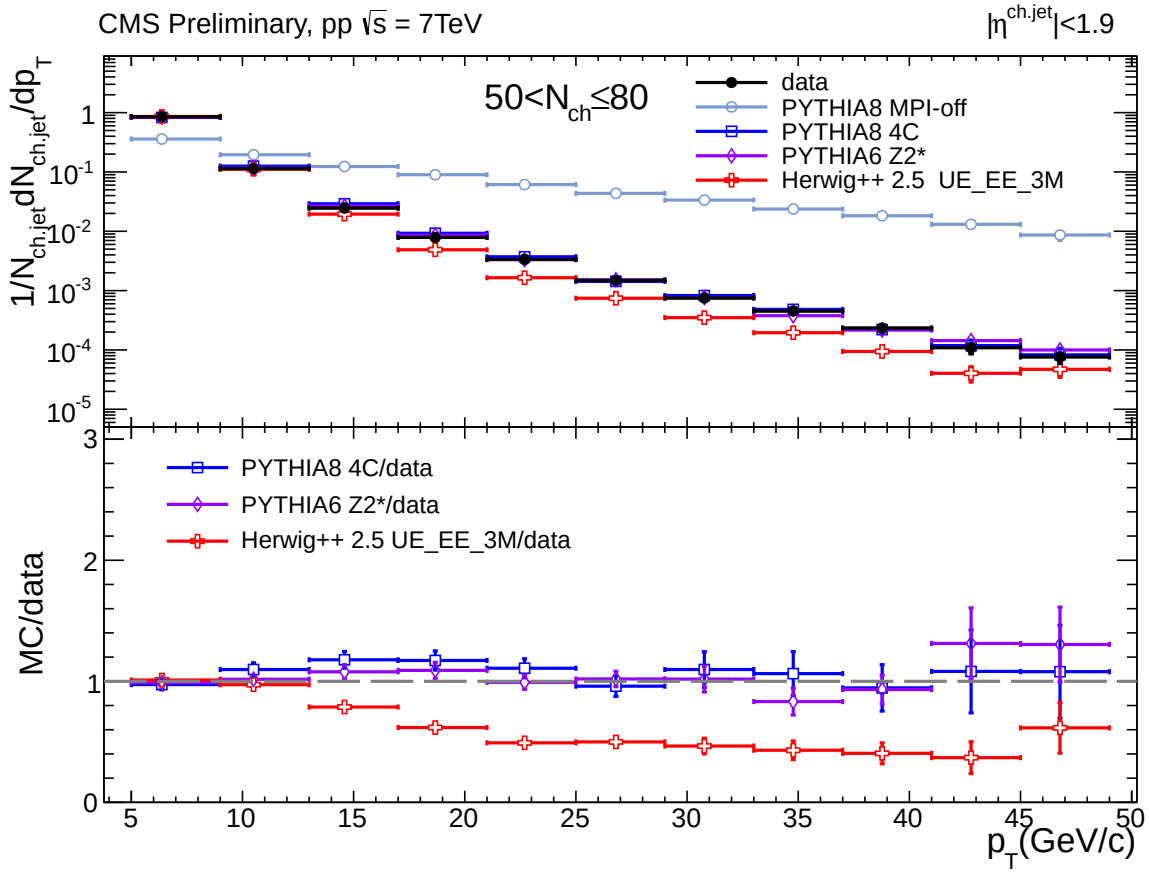

Figure 14: Inclusive charged-particle jet p_{T} spectrum in the multiplicity domain $50 < N_{\mathrm{ch}}(|\eta| < 2.4) \leq 80$ in p-p collisions at 7 TeV..

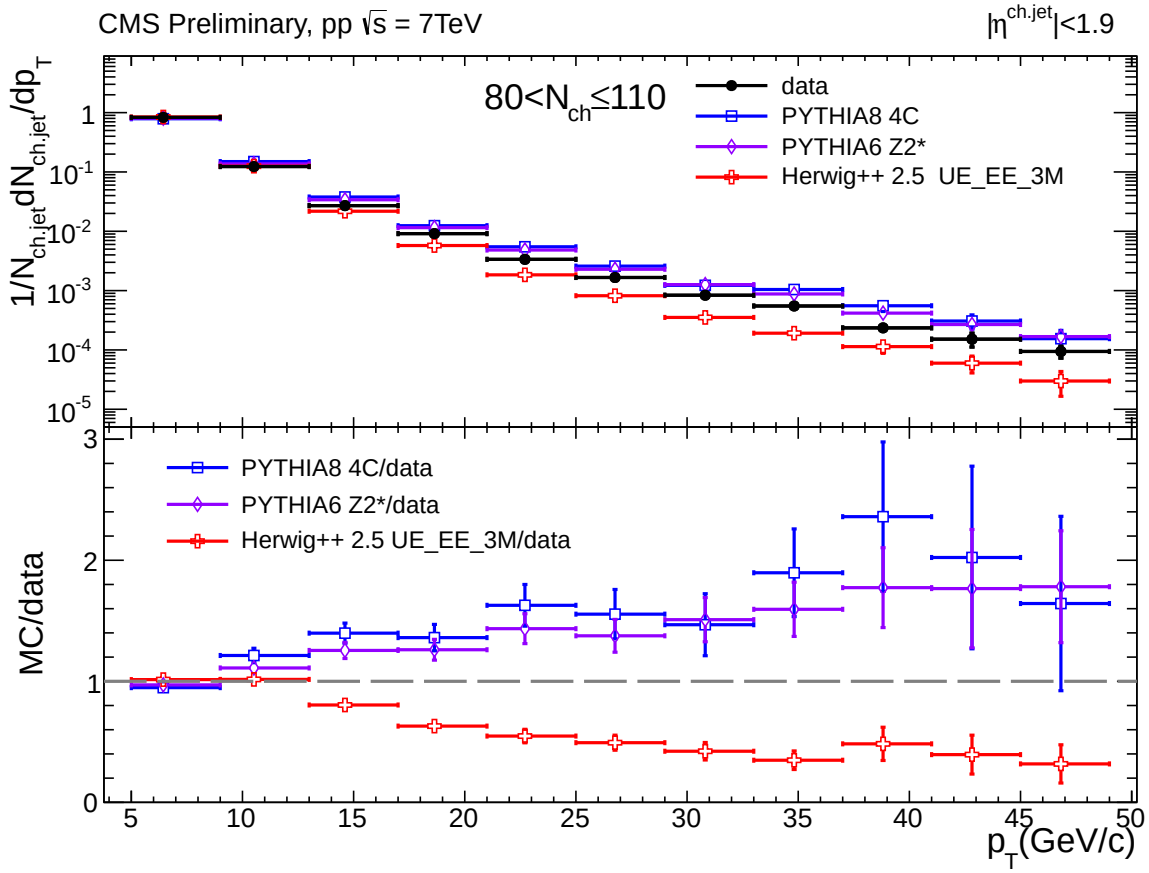

Figure 15: Inclusive charged-particle jet p_{T} spectrum in the multiplicity domain $80 < N_{\mathrm{ch}}(|\eta| < 2.4) \leq 110$ in p-p collisions at 7 TeV..

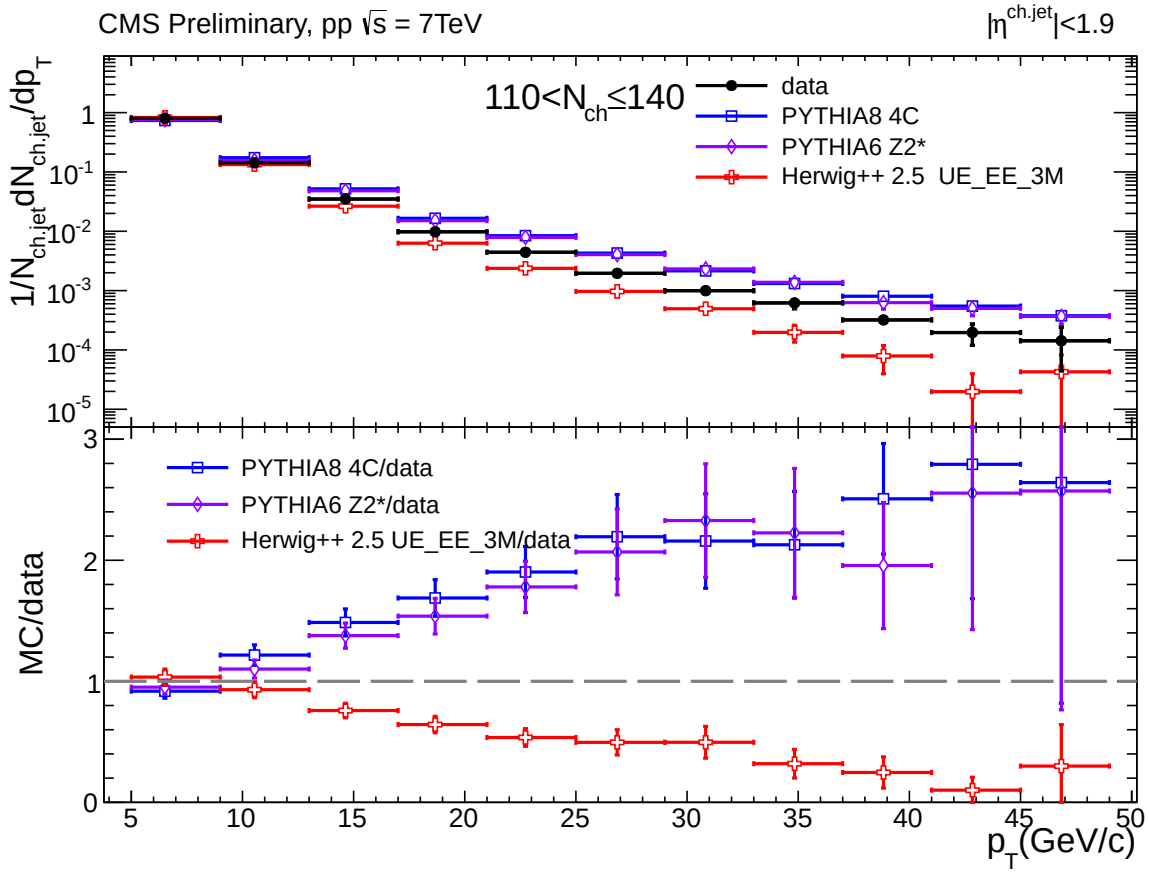

Figure 16: Inclusive charged-particle jet p_{T} spectrum in the multiplicity domain $110 < N_{\mathrm{ch}}(|\eta| < 2.4) \leq 140$ in p-p collisions at 7 TeV..

8.2.3 Charged-particle jet widths

The jet width provides important information to characterize the internal jet radiation dynamics. We study it quantitatively through the p_{T} charged-track density in ring zones with respect to the jet center, defined as:

$$\rho = \left\langle \frac{1}{p_{\mathrm{T}}^{\mathrm{ch.jet}}} \frac{dp_{\mathrm{T}}^{tracks}}{dR} \right\rangle_{\mathrm{ch.jets}}, \tag{3}$$

where $R = \sqrt{(\phi - \phi_{\mathrm{jet}})^2 + (\eta - \eta_{\mathrm{jet}})^2}$ is the distance of each track to the jet axis. Jets with $p_{\mathrm{T}}^{\mathrm{ch.jet}} \geq 5$ GeV/c are selected for the study. The data and MC predictions are compared in the five multiplicity intervals in Figs. 17–21. The low-multiplicity events jets are significantly narrower than predicted by PYTHIA and HERWIG, whereas in the high multiplicity events they are of comparable width as in the MCs. The dependencies shown in Figs. 17–21 actually indicate that both PYTHIA and HERWIG underestimate the evolution of jet width with multiplicity. In particular, the pattern observed in the data indicates that the models need to be readjusted to reproduce the activity in the innermost ring of the jet as a function of event multiplicity.

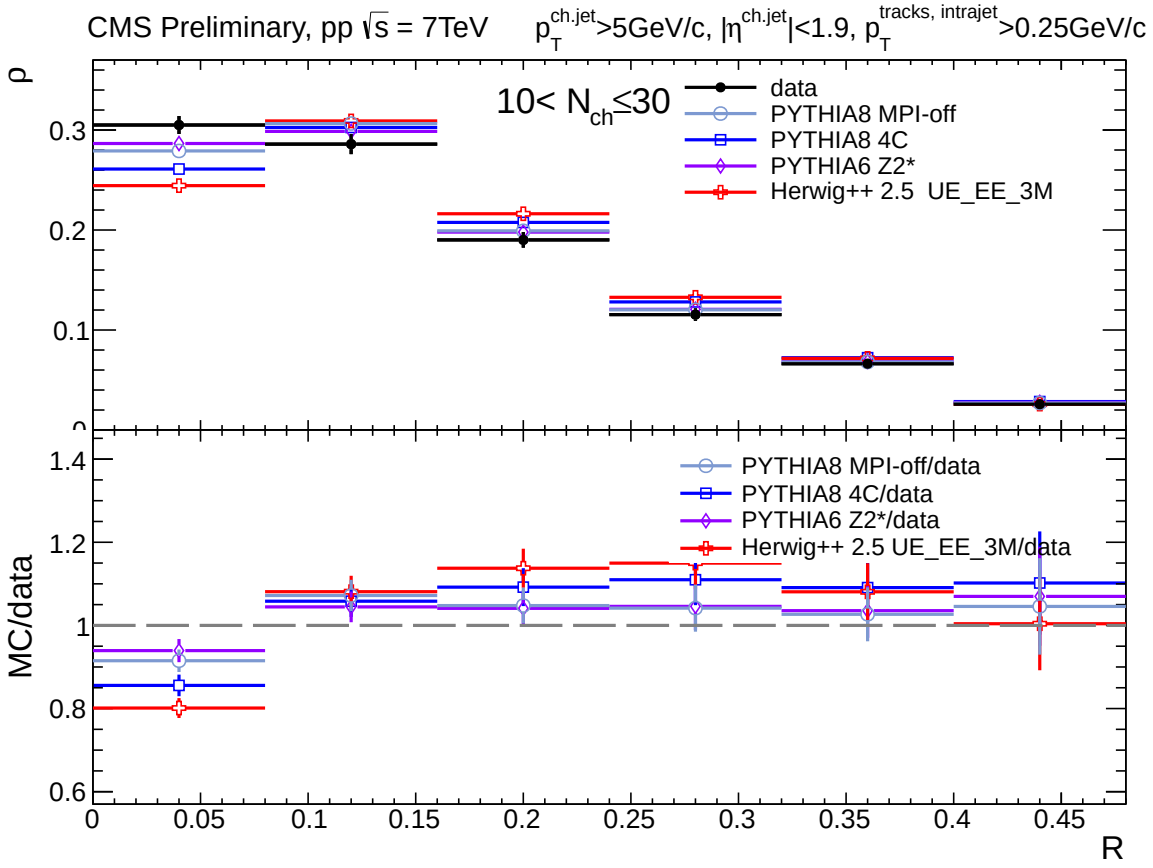

Figure 17: Charged-particle jet p_{T} density in ring zones as a function of distance to the jet axis R, Eq. (3), in the multiplicity domain $10 < N_{\mathrm{ch}}(|\eta| < 2.4) \leq 30$ in p-p collisions at 7 TeV..

9 Conclusions

The characteristics of particle production in p-p collisions at $\sqrt{s} = 7$ TeV have been studied as a function of the event charged-particle multiplicity (N_{ch}) by separating the measured tracks

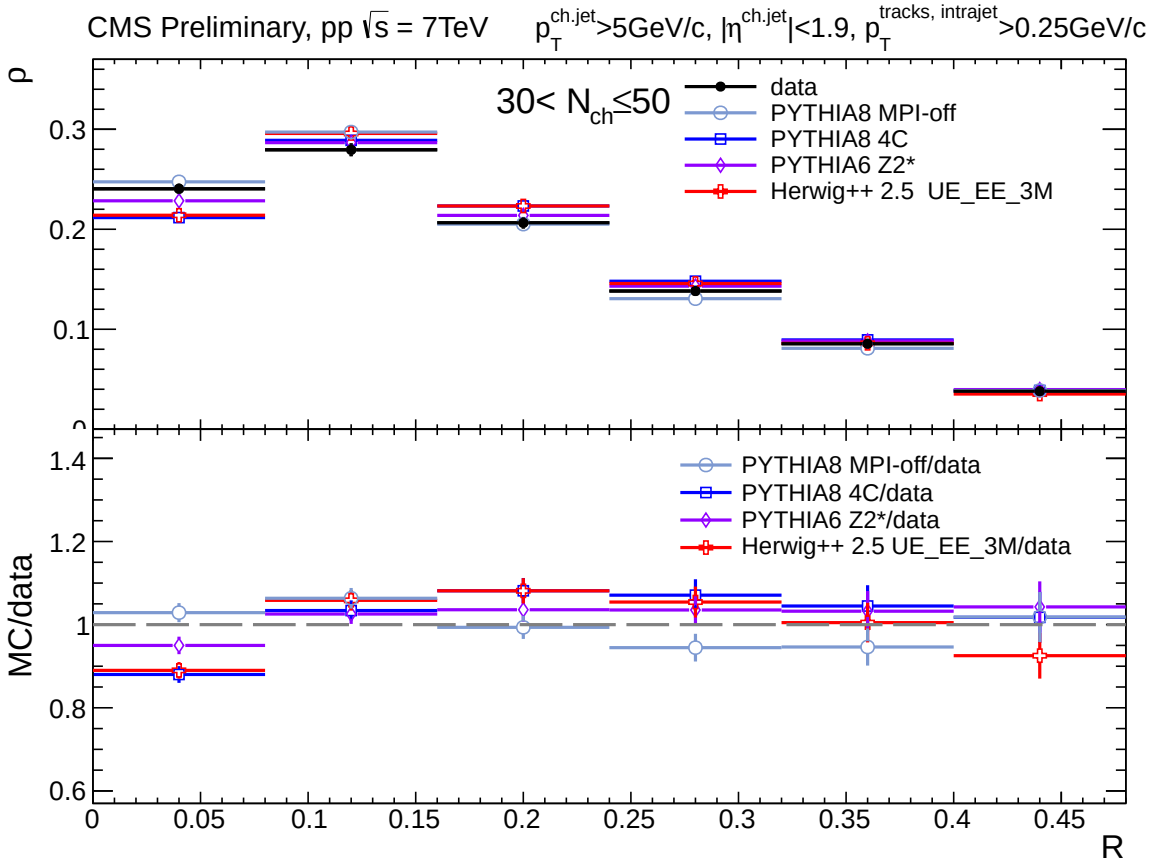

Figure 18: Charged-particle jet p_{T} density in ring zones as a function of distance to the jet axis R, Eq. (3), in the multiplicity domain $30 < N_{\mathrm{ch}}(|\eta| < 2.4) \leq 50$ in p-p collisions at 7 TeV..

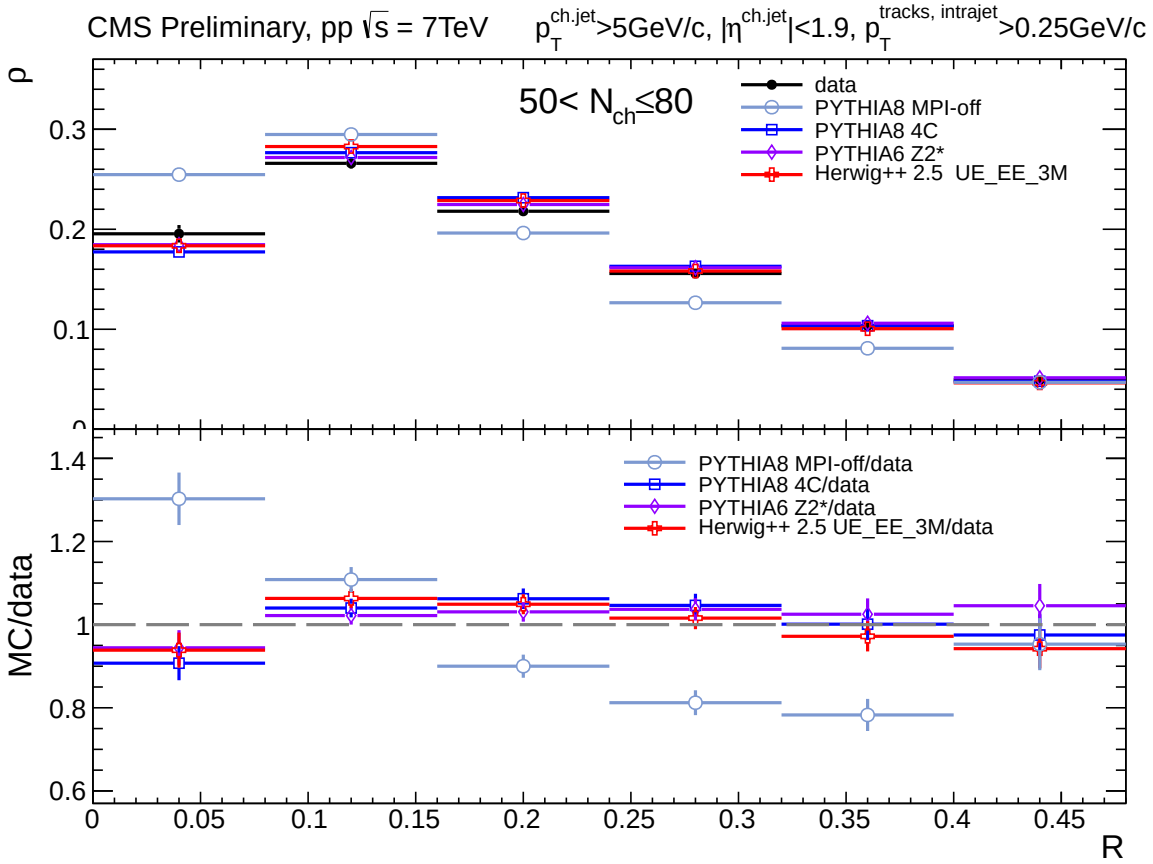

Figure 19: Charged-particle jet p_{T} density in ring zones as a function of distance to the jet axis R, Eq. (3), in the multiplicity domain $50 < N_{\mathrm{ch}}(|\eta| < 2.4) \leq 80$ in p-p collisions at 7 TeV..

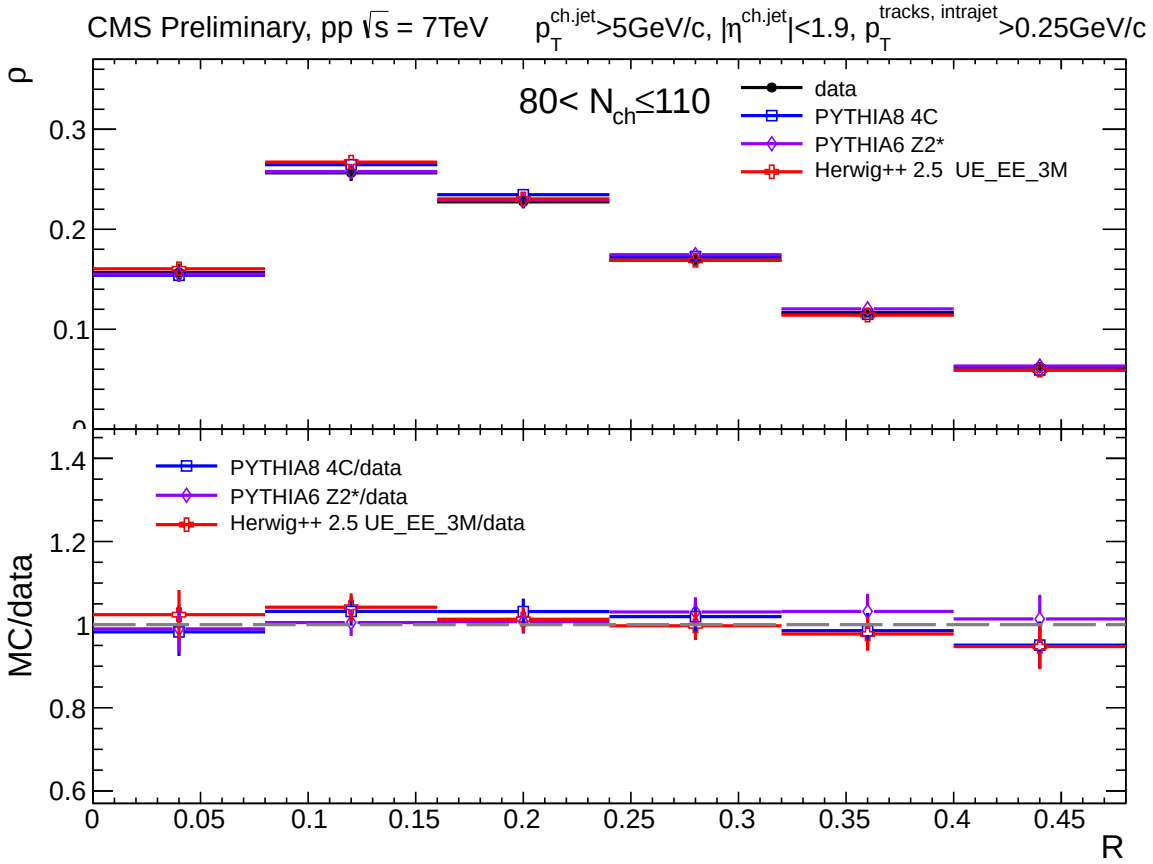

Figure 20: Charged-particle jet p_{T} density in ring zones as a function of distance to the jet axis R, Eq. (3), in the multiplicity domain $80 < N_{\mathrm{ch}}(|\eta| < 2.4) \leq 110$ in p-p collisions at 7 TeV..

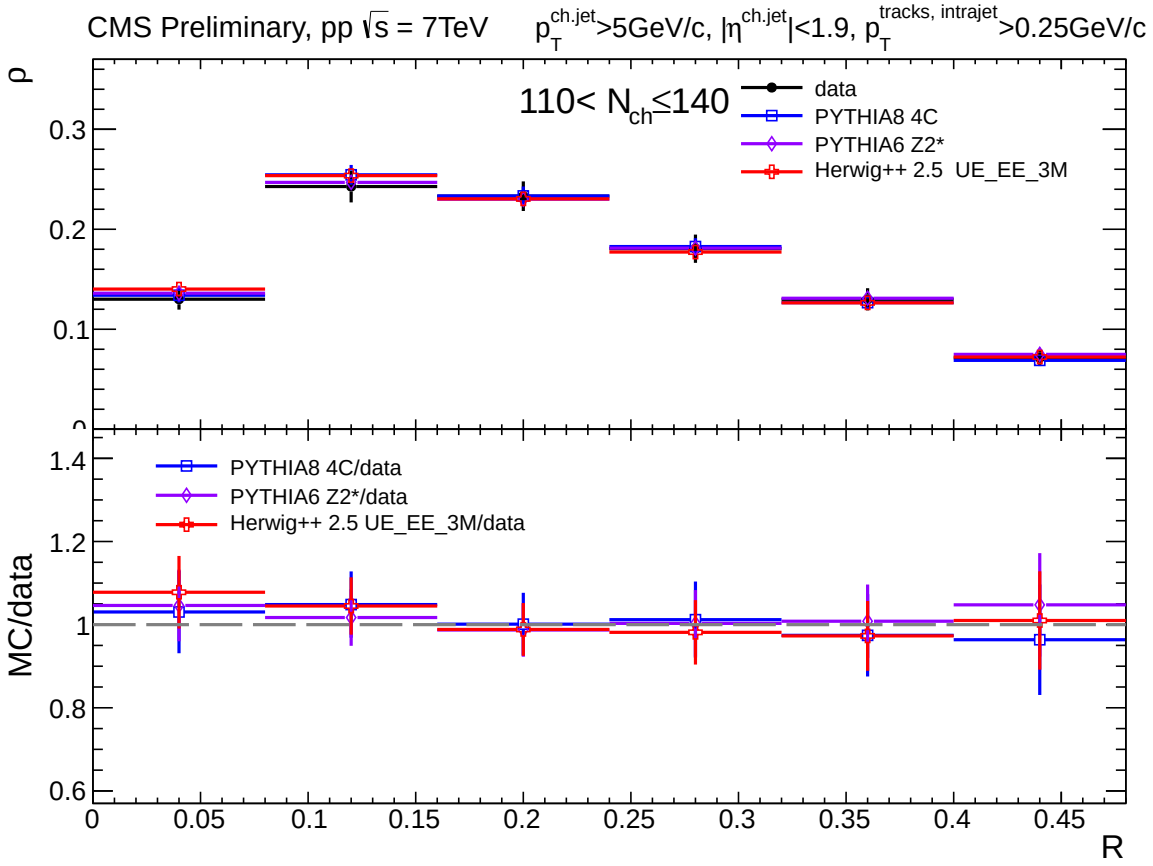

Figure 21: Charged-particle jet p_{T} density in ring zones as a function of distance to the jet axis R, Eq. (3), in the multiplicity domain $110 < N_{\mathrm{ch}}(|\eta| < 2.4) \leq 140$ in p-p collisions at 7 TeV..

into those belonging to jets and those belonging to the underlying event (UE). Charged tracks are measured within pseudorapidity $|\eta| < 2.4$ above transverse momenta $p_{\mathrm{T}} = 0.25$ GeV/c and charged-particle jets are reconstructed above $p_{\mathrm{T}} = 5$ GeV/c with track-only information. The distributions of jet p_{T}, average p_{T} of UE tracks and jets, jet rates, and jet shapes are studied as a function of N_{ch} and are compared to the predictions of the PYTHIA and HERWIG Monte Carlo (MC) event generators.

The mean transverse momenta of all tracks in the event, $\langle p_{\mathrm{T}}^{\mathrm{track}} \rangle$, as well as those from the UE tracks alone, $\langle p_{\mathrm{T}}^{\mathrm{UE}} \rangle$, show a slow (logarithmic) increase on N_{ch}, which is well described by both PYTHIA tunes but not properly described by HERWIG++, which shows softer average p_{T} with larger N_{ch}, and it is completely missed by PYTHIA8 without MPI which predicts too hard transverse momenta at increasing multiplicities. The N_{ch}-dependence of the transverse momenta of intrajet constituents and leading-track of the jet shows the opposite behaviour compared to those from the global and underlying events and decreases logarithmically with increasing multiplicities.PYTHIA6 tune Z2* describes this behaviour quite well and somewhat better than HERWIG++ whereas PYTHIA8 tune 4C produces harder intrajet charged particle spectrum at high multiplicities, and PYTHIA8 (MPI-off) again completely misses the data since it cannot enrich the high-multiplicity events with semi-hard parton scattering activity.

The per-event charged-particle jet rates have been studied as a function of N_{ch} for semihard ($p_{\mathrm{T}} > 5$ GeV/c) and hard ($p_{\mathrm{T}} > 30$ GeV/c) jets. For the semihard cutoff, we measure averages of about 0.5 jets/event to about 4 jets/event going from the lowest to the highest charged-particle multiplicity. Such results are very well described by PYTHIA6 tune Z2*, while predictions of PYTHIA8 tune 4C overestimate the rates at all N_{ch} and HERWIG 2.5 underestimates them for increasing N_{ch}. For the higher 30 GeV/c cutoff, a large data-MC disagreement is found in the higher multiplicity bins with both versions of PYTHIA predicting factor of two more jets than seen in the data and HERWIG predicting a factor of 10 less jet rates than experimentally measured. Predictions without multi-parton interactions fail completely to describe the data.

As the event-multiplicity increases, PYTHIA systematically predicts harder p_{T} spectra than seen in the data, whereas HERWIG shows the opposite trend. The study of the jet-width as a function of multiplicity is, on the other hand, well described in general for high-multiplicity events by both MC generators which, however, predict but wider jets in the lowest-multiplicity events than seen in the data.

We have demonstrated that many features of event multiplicity dependence of the jet and UE properties, in particular the jet ones, differ from the MC predictions. In general, PYTHIA reproduces better the data than HERWIG for all observables measured. Of special interest is the large difference between the jet p_{T} spectra in the data and in the MC predictions for the two highest multiplicity bins (showing good agreement in first three multiplicity domains). Jets are softer and less abundant there which explains the observed larger sphericity of high multiplicity events at the LHC compared to PYTHIA estimates. The Monte Carlo predictions also fail to describe intrajet spectra. The deviation of MC predictions from the data for the spectra of leading intrajet particles is not big but can be characterized by a systematic pattern. At the same time the characteristics of the UE are well reproduced by some of the MC simulations in all the multiplicity domains considered.

The results obtained in this study are of importance for both improving the description of data by MC generators and getting a firmer grasp on the fundamental mechanisms of multiparticle production. The present state-of-the-art event generator tuned to reproduce the minimum-bias LHC data cannot describe differentially within a single model the dependence of various quantities on event multiplicity – especially in the high multiplicity range where, e.g. PYTHIA

produces many particles because of having too many jets and HERWIG seems to contain too many soft multiple scatterings. However, taken together the MC predictions bracket the data pointing to possible ways for successful tuning of the present MC generators by improving, in particular, the description of the soft and semi-hard dynamics implemented in the models of multiple parton interactions. In this light, results of the PYTHIA 8 with switched-off MPIs are very demonstrative, showing that there is no way to reproduce the characteristics of the jet and underlying event data for moderate and large particle multiplicities ($N_{\rm ch} > 20$ within $|\eta| < 2.4$), without such extra mechanism of particle production.

References

[1] Yu.L. Dokshitzer et al., "Basics of Perturbative QCD", Editions Frontiers, 1991

[2] P. Bartalini and L. Fano, (eds.), "Multiple partonic interactions at the LHC. Proceedings, 1st International Workshop, MPI'08, Perugia, Italy, Oct. 2008"; arXiv:1003.4220 [hep-ex].

[3] V.P. Shelest, A.M. Snigirev, G.M. Zinovjev, Phys. Lett. **B113** (1982) 325

[4] T. Sjöstrand et al., Phys. Rev. D36 (1987) 2019

[5] I.M. Dremin, V.A. Nechitailo, Phys. Rev. D **84**, 034026 (2011); **70**, 034005 (2004).

[6] M. Ryskin, A. Snigirev, Phys. Rev. D83 (2011) 114047

[7] M. Ryskin, A. Snigirev, Phys. Rev. D83 (2012) 014018

[8] M. Diehl, D. Ostermeier, A Schaefer, JHEP **1203** (2012) 089

[9] B. Block, Yu. Dokshitzer, L. Frankfurt, M. Strikman, Eur. Phys. Jour. **C72** (2012) 1963

[10] T. Sjöstrand, S. Mrenna, P. Skands, JHEP **0605** (2006) 026.

[11] T. Sjöstrand, S. Mrenna, P. Skands, Comput. Phys. Commun. **178** (2008) 852

[12] S. Gieseke *et al.*, *Herwig++ 2.5 Release Note*, arXiv1102.1672

[13] CMS Collaboration, V. Khachatryan et al., JHEP **1101** (2011) 079.

[14] CMS Collaboration, V. Khachatryan et al., JHEP **1009** (2010) 091.

[15] A. Velasquez, arXiv:1110.2278

[16] ALICE Collaboration, Eur. Phys. J. C (2012) 72:2124.

[17] ATLAS Collaboration, arXiv:1207.6915.

[18] ATLAS Collaboration, arXiv:1206.2135.

[19] CMS Collaboration, Phys. Lett. B 699 (2011) 48.

[20] R. Corke, T. Sjöstrand, JHEP **1103** (2011) 032.

[21] B. Andersson, G. Gustaffson, G. Ingelman, T. Sjöstrand, Phys. Rept. **97** (1983) 31.

[22] CMS Collaboration, V. Khachatryan et al., JINST **0803** (2008) S08004.

[23] V. Khachatryan et al. (CMS Collaboration), JHEP 02 (2010) 041.

[24] CMS Collaboration, V. Khachatryan et al., Eur. Phys. J. C **70** (2010) 555; CMS-QCD-10-010-002.

[25] M. Cacciari, G. Salam, and G. Soyez, The anti-kt jet clustering algorithm, JHEP **0804** (2008) 272.

[26] CMS Collaboration, S. Chatrchyan et al., JHEP 01 B **079** (2011) 30.

[27] CMS Collaboration, V. Khachatryan et al., arXiv:1204.3170; QCD-10-029.

[28] CMS Collaboration, V. Khachatryan et al., CMS PAS TRK-10-005.

[29] CMS Collaboration, V. Khachatryan et al., Nucl. Instrum. Meth. **A582** (2007) 781.

[30] CMS Collaboration, "Performance of Jet Reconstruction with Charged Tracks only", CMS AN-2008/041.

[31] G. DAgostini, Nucl. Inst. Meth **A326** (1995) 487.